8-2023

Multiphysics Diesel Aftertreatment System Modeling for Reduced Emissions from Hybrid Electric Heavy-Duty Powertrains

Uday Srivastav
usrivas@clemson.edu

MULTIPHYSICS DIESEL AFTERTREATMENT SYSTEM MODELING FOR REDUCED EMISSIONS FROM HYBRID ELECTRIC HEAVY-DUTY POWERTRAINS

A Thesis
Presented to
the Graduate School of
Clemson University

In Partial Fulfillment
of the Requirements for the Degree
Master of Science
Automotive Engineering

---

by
Uday Srivastav
August 2023

Accepted by:
Dr. Robert Prucka, Committee Chair
Dr. Qilun Zhu, Co-chair
Dr. Benjamin Lawler

ABSTRACT

Hybridization of heavy-duty on-road vehicles presents an opportunity to significantly reduce internal combustion engine emissions in real-world operation. These gains can be realized through the coordination of the electric drive, engine, and aftertreatment systems. Accurate Multiphysics models of all powertrains sub-systems are required to achieve the goal of reduced emissions. This research aims to develop a model of a highly complex diesel engine aftertreatment system. This study focuses on utilizing transient data for calibration and validation of the aftertreatment system and reducing the run time when compared to real-time experiments. The calibration focuses on two physical phenomena, thermal behavior and chemical kinetics. Once a base model is set up, the calibration parameters are optimized using an accelerated genetic algorithm for factors that contribute to the reaction rates and the exhaust gas temperature. The research only utilizes data from transient engine experiments to better automate and speed-up the calibration process over traditional methodologies.

The model setup ensures that it is fast-running, with ten times speed-up as compared to real-time. The model is capable of predicting and matching combined error for CO and NO_x concentration on a cumulative basis under 9.8% and 1% for the experimental data for cold FTP and hot FTP, respectively. The results of the model also predict close trends with the temperature profiles and have a close match with the tailpipe emission species concentration over a cumulative basis but fails to capture some transient behavior. The model results are also evaluated to identify the leading cause for the error

so the model can be improved for further development. The model has the capability to generate results for the aftertreatment for further research.

ACKNOWLEDGMENTS

With immense gratitude, I extend my heartfelt appreciation to the remarkable individuals who have played a crucial role in making this thesis a reality.

To Dr. Robert Prucka, my thesis supervisor, I am deeply indebted for their unwavering support, invaluable guidance, and constant encouragement throughout this transformative research journey.

In the same breath, I sincerely thank Dr. Qilun Zhu and Dr. Benjamin Lawler for their brilliant insights and constructive feedback that have shaped this thesis into its present form. Their mentorship has been a beacon of inspiration.

I would like to acknowledge the support and assistance provided by the research group members at Clemson, especially Erik Vorwerk, for constantly supporting in various stages of this research. Their contributions have significantly improved the quality of this work.

My heartfelt appreciation also extends to my beloved parents and family for their unyielding support and the privilege to pursue my dreams abroad. Your love and belief in me have been my driving force. To my dear friends and Helly, your unwavering encouragement and belief in my abilities have been a constant source of strength, motivating me to overcome challenges and strive for excellence.

To everyone, whether you offered a word of encouragement, a helping hand, or a listening ear, I extend my deepest thanks. Each of you has left an indelible mark on my academic journey and personal growth.

TABLE OF CONTENTS

Page

LIST OF TABLES

Page

LIST OF FIGURES

Page

INTRODUCTION

Automotive Pollution

Internal combustion engines are a significant source of air pollution due to vehicle tailpipe emissions. The percentage of air pollution due to internal combustion engines can vary depending on the specific location and the types of sources of pollution present. Internal combustion engines, however, play a sizable role in worldwide air pollution.

Since 1990, the transportation industry has had the most considerable increase in GHG emissions of any other industry. The Environmental Protection Agency (EPA) estimates that in 2021, transportation accounted for around 29% of all GHG emissions in the United States[1]. The growth in vehicle travel, particularly in personal vehicles, is the leading cause of this increase in transportation emissions[2].

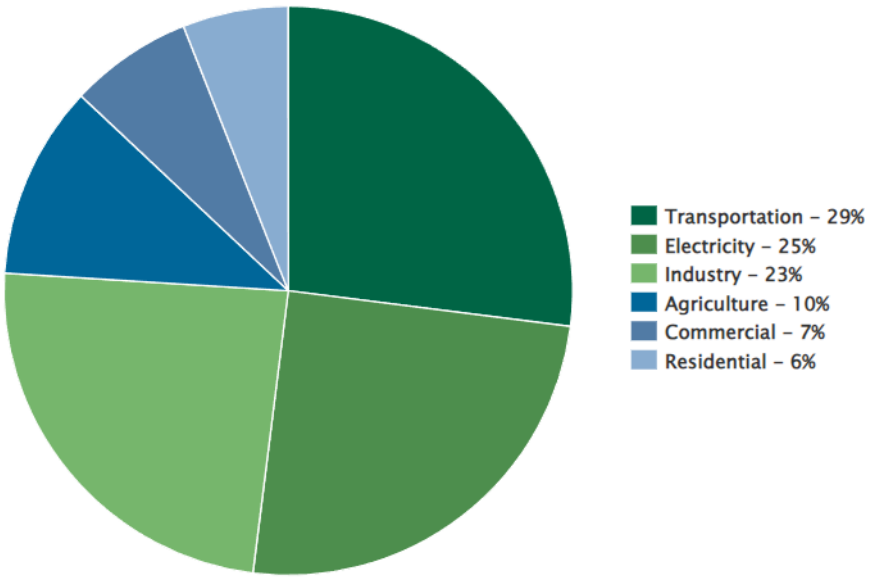

Figure 1: 2021 US GHG Distribution

The pollutants such as carbon dioxide (CO2), methane (CH4), and nitrous oxide (NOx) emissions are associated with transportation-related vehicles, such as cars, trucks, buses, and airplanes. Passenger automobiles and light-duty trucks are the main contributors to transportation-related GHG emissions, accounting for more than 55% of all emissions. Medium and heavy-duty trucks, buses, ships, and trains are further sources[3].

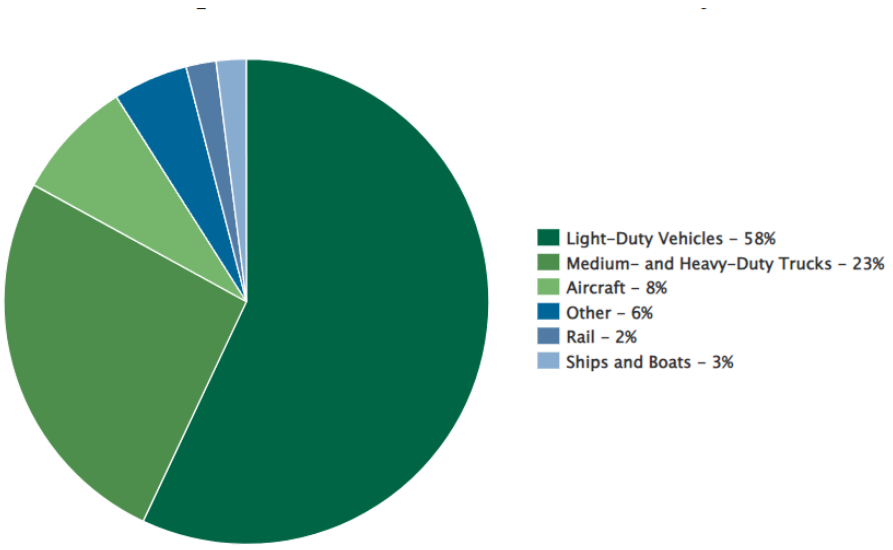

Figure 2: 2021 US GHG Distribution for Transportation Sector

Many different techniques have been suggested and implemented to address transportation related GHG emissions. Increasing the usage of low-emission vehicles like hybrid, electric, and fuel-cell vehicles is one option. There have also been initiatives to increase vehicle fuel efficiency, such as establishing fuel economy standards and encouraging the use of biofuels. However, considerable work still needs to be done to

minimize GHG emissions associated with transportation and lessen the effects of climate change.

Automotive Pollution Regulation and Norms

Since automotive emissions are a big concern worldwide, many organizations are in place that regulates and impose strict standards. The Environmental Protection Agency (EPA) and the California Air Resources Board (CARB) are two prominent regulatory organizations in the US that considerably impact air quality control and environmental protection, notably concerning automobile emissions. The Environmental Protection Agency (EPA) is a federal organization in charge of establishing and upholding national environmental protection rules in the US, particularly those pertaining to car emissions. A waiver from the EPA allows the California Air Resources Board (CARB), a state agency in California, to set stricter car emissions requirements. The requirements of CARB, often known as the California Low Emission (LEV) program, are more stringent than the federal standards.

Additionally, CARB encourages the use of zero-emission cars (ZEVs) and has established goals for automakers to build and market a specific proportion of ZEVs in California. The Zero Emission Vehicle Mandate is the name given to this regulation. Other states may comply with either federal EPA regulations or stricter CARB standards.

EPA finalized new NO_X, PM, HC, and CO emission standards for heavy-duty compression-ignition engines.

Model year	NO x (mg/hp-hr)	HC (mg/hp-hr)	PM (mg/hp-hr)	CO (g/hp-hr)
2027 and later	**35	60	5	6

Table 1: Final Drive Cycle Emissions Standards for Light HDE, Medium HDE, and Heavy HDE over the RMC SET and FTP Drive Cycle[4]

Model year	NO x (mg/hp-hr)	HC (mg/hp-hr)	PM (mg/hp-hr)	CO (g/hp-hr)
2027 and later	**50	140	50	6

Table 2: Final Drive Cycle Emissions Standards for Light HDE, Medium HDE, and Heavy HDE over the LLC Drive Cycle[4]

**An interim NO x compliance allowance of 15 mg/hp-hr applies for any in-use Medium HDE and Heavy HDE testing. Manufacturers will add the compliance allowance to the NO x standard that applies for each duty cycle and for off-cycle Bin 2, for both in-use field testing and laboratory testing as described [5]

The final standards for the FTP and LLC are 80 to 90 percent, or more, lower than current standards, which will contribute to reductions in emissions under low power operations and under cold-start conditions. Phase 3 of the EPA GHG Emission standards, introduced in April 2023, poses stricter emissions norms over the MY2027. The EPA also plans on adapting the CARB's LLC drive cycle.

Weight Class	Drive Cycle	CO_2 Standards (g/mi)	Annual Reduction Rate (MY2028 and later)
Class 2b-5	Urban	453	4 %
Class 6-8	Urban	1029	4.5 %
Class 2b-8	Highway	579	4 %

Table 3: Proposed Phase 3 (MY2028) Regulations[6]

Diesel Emissions

Emissions from the CI diesel engine can vary across the load and the equivalence ratio. Based n the operation region of the engine formation, pollutants can be showcased in a broad spectrum. Since diesel engines operate very lean, the primary concern is the

formation of soot and NOx, an excess species in the exhaust gas. Hence to tackle and reduce these emissions variety of devices were implemented to reduce the emissions species. The advancement of aftertreatment devices is needed to address the increasingly strict emission standards.

Diesel Aftertreatment System

Aftertreatment means relating to a catalytic converter, particulate filter, or any other system, component, or technology mounted downstream of the exhaust valve (or exhaust port) whose design function is to decrease emissions in the engine exhaust before it is exhausted to the environment. Exhaust gas recirculation (EGR) and turbochargers are not aftertreatment; they work to reduce engine-out emissions before the aftertreatment system. Additionally, these engine technologies do not lower engine-out emissions to a level below the regulated standards. This highlights the importance of aftertreatment systems for diesel engines and the complexity of their design. With the increasing focus on reducing harmful emissions from diesel engines, OEMs have invested heavily in developing effective aftertreatment solutions. These systems are critical for meeting the stringent emission norms set by the EPA and other regulatory bodies.

The complexity of aftertreatment systems for diesel engines stems from the fact that these engines produce significant amounts of particulate matter (PM) and nitrogen oxides (NOx), both of which are harmful to human health and the environment. While a three-way catalyst (TWC) converter is effective for treating the emissions from gasoline engines, it is not sufficient for treating the emissions from a diesel engine since stoichiometric air-to-fuel ratio operation is not possible due to excessive soot production.

Diesel engines require a more complex aftertreatment system that can effectively reduce CO, PM and NO_x in an exhaust environment that is oxygen rich, from lean operation, and allow relatively low temperature, due to high engine efficiency. To achieve this, aftertreatment systems for diesel engines typically use a combination of technologies, including diesel oxidation catalyst (DOC), diesel particulate filters (DPFs), and selective catalytic reduction (SCR). These systems may also require the use of additional reductants, such as urea, to effectively reduce NOx emissions.

Overall, the design of aftertreatment systems for diesel engines is complex and requires a deep understanding of the combustion process and the chemistry of emissions. As emission standards continue to become more stringent, OEMs will need to continue investing in research and development to stay ahead of the curve and ensure compliance with regulations.

Close-Packaged Aftertreatment Systems

Close-packaged aftertreatment refers to a comprehensive emissions control system for diesel engines that combines multiple emission control technologies into a single unit. It integrates various components, such as diesel particulate filters (DPFs), selective catalytic reduction (SCR) systems, and diesel oxidation catalysts (DOCs), into a compact and efficient package. Integrating multiple emission control technologies into a single unit optimizes space utilization, simplifies installation, and reduces overall costs.

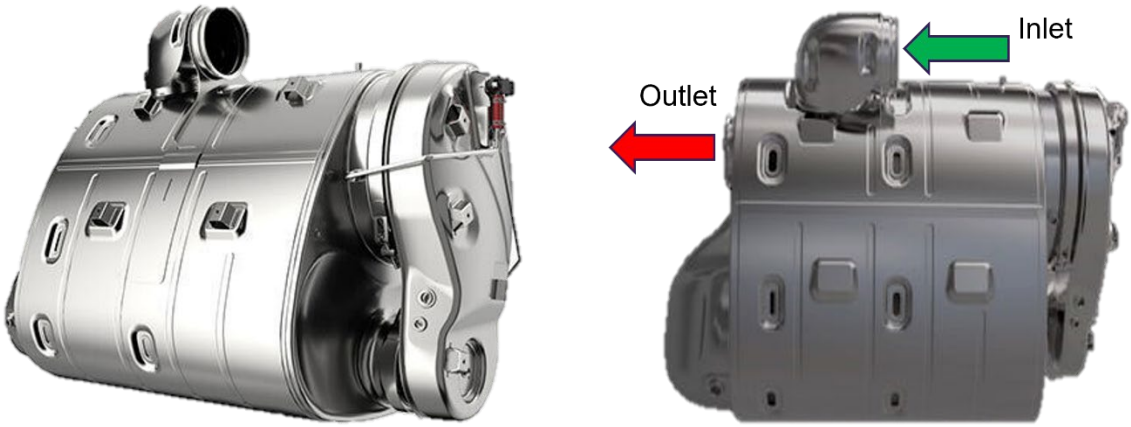

Figure 3: An example of a close-packaged aftertreatment system[7]

This relatively newer architecture for the aftertreatment pieces layout is the one box where the components are placed in the best order to reduce emissions. Still, it may not be arranged along the same axis, i.e., the placement of each catalyst brick is in a fashion to make the system more compact. This also ensures better thermal stability by entrapping the heat from the exhaust gas to naturally maintain the temperature and pressure across the catalyst bricks to perform better. The close-packaged system's compact design enhances heat management and retention, leading to better active or forced regeneration and greater passive regeneration.

Close-packaged aftertreatment systems have become increasingly common in modern diesel engines, particularly in heavy-duty and medium-duty applications. They play a vital role in reducing diesel emissions, improving air quality, and meeting stringent emission standards set by regulatory agencies worldwide.

Objectives

The key objectives of this thesis project are to understand the modeling and calibration methods for a complex Multiphysics aftertreatment system in modeled using GT-Suite, which can be used to develop similar aftertreatment systems in the future.

- Development of a high-fidelity fast-running model.
- Design a 1D GT-Suite model to capture thermal behavior and chemical kinetics.
- Characterization of ATS a gray box to calibrate unknown parameters
- Analyzing and processing transient experimental data sets for input parameter tuning
- Characterization of governing chemical kinetics for surface reactions of each ATS component to match experimental data.
- Model calibration using only transient experimental data to try to automate the process as much as possible.
- Predict tailpipe CO and NO_x concentration.
- Validation of the ATS over cold FTP and hot FTP drive cycles.
- Analysis of the ATS for heavy-duty hybrid vehicle operation.

THEORY AND BACKGROUND

Substrate

The substrate is the catalyst part responsible for increasing the surface area within the catalyst bricks. The substrates can have a variety of layouts or structures, like hexagons, honeycombs, squares, etc.[8]. The thermal properties of the substrate for typical aftertreatment bricks are cordierite or silicon carbide. Primarily cordierite is used as non-metallic substrates for catalyst bricks, silicon carbide for DPFs, and carbon or stainless steel for metallic substrates.

Washcoat

The thermal properties of the washcoat are identical to alumina, as the Pt or Vd catalysts are infused with alumina and coated over the substrate to form a layer of catalyst washcoat. In some cases, multiple washcoat layers are added to improve efficiency by increasing the surface area and catalyst activity. The diffusion properties are mandatory to replicate multiple layers of washcoat. The pore diffusion occurs over the washcoat surface to react with the active catalyst sites. The catalyst sites on continuous reactions are prone to poisoning, reducing the active site density and efficiency[9], [10]. The washcoat layer can be present in various forms, like in the zone-coated catalyst bricks, which have multiple types of washcoat in different catalyst or substrate surface zones[11].

The washcoat may lose its efficiency and affect the performance of the catalyst, this is known as ageing or poisoning of the catalyst.

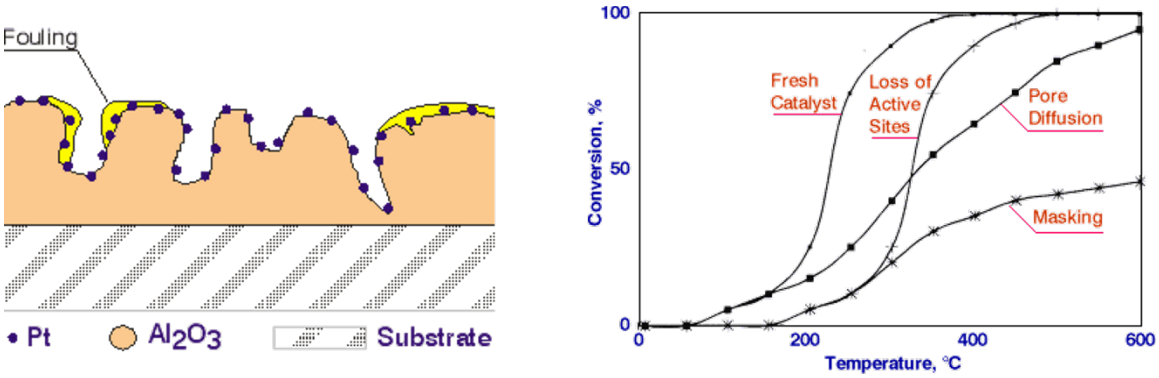

Figure 4: Poisoning of Washcoat[12]

The figure 4. depicts the poisoning of the active sites over the washcoat [13]. Over time, due to exposure to harsh reaction conditions or contaminants, some of these active sites may become deactivated or blocked, reducing the catalyst's overall activity. Catalysts often have a porous structure, however, as the catalyst ages, these pores may become clogged or blocked by reaction by-products or other substances. This pore diffusion limitation can slow down the rate at which reactants can access the active sites, leading to reduced catalytic efficiency[14]. In some cases, undesired by-products or residues from the reaction can accumulate on the catalyst's surface, covering or "masking" some of these active sites.

Diesel Oxidation Catalyst (DOC)

The diesel oxidation catalyst (DOC) is primarily used to oxidize NO, CO, and HC[8]. The reactions that take place in the DOC are exothermic in nature, i.e., the reactions contribute to the gain in exhaust gas temperature in the DOC[8]. Oxidation of CO results in the highest heat loss due to higher enthalpy of formation for CO_2. The DOC is primarily made of a ceramic or metallic substrate with an alumina washcoat loaded

with catalysts[15]. The washcoat serves to enhance the conversion efficiency of the DOC. The washcoat of the DOC typically consists of platinum group materials (PGM). For catalysts, platinum (Pt) and palladium (Pd) are generally used. The ratio of the metals directly affects the Active Site Density (ASD) of the catalyst, which affects the performance of the DOC. In past research, it was observed that DOCs that have Pt and Pd catalysts perform better when compared to just Pt catalysts [16].

The primary reactions associated with the DOC are:

$$2CO + O_2 \rightarrow 2CO_2$$

$$2NO + O_2 \rightarrow 2NO_2$$

$$2C_3H_6 + 9O_2 \rightarrow 6CO_2 + 6H_2O$$

These reactions indicated oxidation of the trace emissions species that are present in the exhaust gas. The DOC is solely responsible for oxidizing the emission species, and the DOC's efficiency is determined by the conversion of NO, CO, and HCs. The oxidation of NO to NO_2 is essential as it is proven that a higher $NO_2{:}NO$ ratio is desirable and results in better performance of the SCR[17].

Diesel Particulate Filter (DPF)

The DPF's main purpose is to filter and retain the soot or particulate matter (PM) present in the exhaust gas. The exhaust gases flow across a highly porous wall or channels, and these channels trap the PM. These channels are ceramic-based substrates and can have a variety of channel shapes as per manufacturers' requirements.

The DPF is generally present downstream of the DOC. In cases where the unburned HCs escape the DOC without being converted, they tend to settle down on the soot particles[8]. Although the concentration is very low, this generally occurs when the engine runs a relatively high fuel/air ratio. Hence the DPF also helps capture the unburned fuel, or HCs settled-over soot particles.

The PM deposition in the DPF increases the pressure drop across the DPF. The steady increase in the pressure drop affects the engine performance by increasing the pressure in the exhaust manifold. Hence for removal of this soot (carbon), the soot is burned or oxidized to CO_2, this process is known as regeneration. There are two ways of renewal active and passive. The active regeneration requires an additional source of heat that assists with oxidizing soot. The heat is generated by excessive injection of diesel fuel to increase exhaust gas temperatures to more than 600° C[18].

The regeneration is enhanced by a catalyst that could be PGM-based, like the other catalysts used in aftertreatment devices. Usage of NO_2 is also observed for oxidation as an alternative to O_2. Passive regeneration requires a catalyzed substrate, which reduces the soot oxidation temperature [19]. However, this will result in a variation in $NO_2{:}NO$ ratio. Hence, the DPF is generally followed by a deNOx catalyst, and SCR or the SCR is integrated with the particulate filter to compact the system [18].

The regeneration's governing equations are:

$$C + NO_2 \rightarrow CO + NO$$

$$C + 2NO_2 \rightarrow CO_2 + 2NO$$

$$2C + O_2 \rightarrow 2CO$$

There also exists ash, a non-combustible component from inorganic materials that may be present in fuel or engine oil. The ash traces accumulate in the DPF, which cannot be burned off through the regeneration process. Hence, periodic cleaning of DPF is required to unclog the filter.

Current DPF technology has a very high filtration efficiency. This efficiency is dictated by the soot loading capacity. The DPF loses its performance if the soot loading limit is reached, which introduces risks of damage and heat retention leading to unfavorable exothermic reactions[20].

Selective Catalyst Reduction (SCR)

Like other pollution abatement devices, SCR consists of a catalyst, a reducing agent, and a control system. The catalyst material for SCR is based on Chabazite, Zeolites, Titanium, Vanadium, etc.[21]–[23]. The reducing agent plays a vital role in determining the performance of the SCR. The primary reducing agent is NH_3, which dozed into the exhaust stream as an aqueous solution of urea, also known as Diesel Exhaust Fluid (DEF) or AdBlue. The DEF contains 67.5% of water and 32.5% of urea by mass[8]. The DEF undergoes hydrolysis under elevated temperatures to produce NH_3 which is an active reduction agent. The chemical reactions after the hydrolysis include the reduction and oxidation of NO_x to N_2 and NO_2 respectively. Adsorption and desorption of NH_3 on the active site of the catalyst, the surface takes place for the reduction reactions[24]. The excess NH_3 is stored within the catalyst, as the catalysts have provision for NH_3 storage. The adsorbed NO_2 and NH_3 react to form nitrogen gas

(N_2) and water vapor (H_2O). The catalyst provides an active surface where the reaction can occur efficiently. The NO_x conversion efficiency of the SCR is higher for higher $NO_2{:}\,NO$ ratio.

The governing equations for chemical reactions withing the SCR are:

$$\mathrm{NH_2CONH_2 + 2H_2O \rightarrow NH_3 + CO2}$$

$$4NO + 4NH_3 + O_2 \rightarrow 4N_2 + 6H_2O$$

$$\mathrm{2NO2 \ + \ 4NH3 + O_2 \ \rightarrow \ 3N2 \ + \ 6H2O}$$

$$\mathrm{2NO + 2NO2 \ + \ 4NH3 + O_2 \ \rightarrow \ 4N2 \ + \ 6H2O}$$

Ammonia Slip Catalyst (ASC)

Since the SCR uses ammonia (NH_3) as a reducing agent another potentially harmful chemical is then introduced into the exhaust stream. The ammonia slip catalyst (ASC) is a device that is used to trap excess (NH_3) in the exhaust stream. This device is complimentary and is added downstream of the SCR. The primary function of ASC is to oxidize excess NH_3 that may have bypassed the SCR [13]. The ASC is also coated with PGM catalysts to improve reaction activity. The ASC is a vital component of the SCR system's performance; ASC allows the SCR to operate at a higher $NH_3{:}\,NO_x$ ratio to improve NO_x conversion efficiency. As a result, some amount of NH_3 escapes, the SCR gets oxidized by ASC. The NH_3 slip downstream of the SCR is determined through sensors, and that information is fed to the controller that dozes DEF into the exhaust stream[25][26].

The governing equations that correspond to the operation of the ASC are:

$$2\mathrm{NH}_3 + 0.5O_2 \rightarrow N_2 + 3H_2O$$

$$2\mathrm{NH}_3 + 2.5O_2 \rightarrow 2NO + 3H_2O$$

$$2\mathrm{NH}_3 + 2NO + 1.5O_2 \rightarrow 2N_2O + 3H_2O$$

$$NO + 0.5O_2 \rightarrow NO_2$$

$$2\mathrm{NH}_3 + 2NO_2 \rightarrow N_2 + N_2O + 3H_2O$$

Mass and Heat Transfer

In the catalyst brick, the mass and heat transfer between the exhaust gas and the substrate occurs axially and radially. As per the film theory, there exists radial diffusion. The gases or emission species diffuse over the boundary surface of the washcoat and further diffuse through the pores on the washcoat. This theory is commonly used to analyze and model mass transfer in various systems, such as absorption, distillation, and chemical reactions [27]. It provides a framework for understanding the transport of molecules between phases.

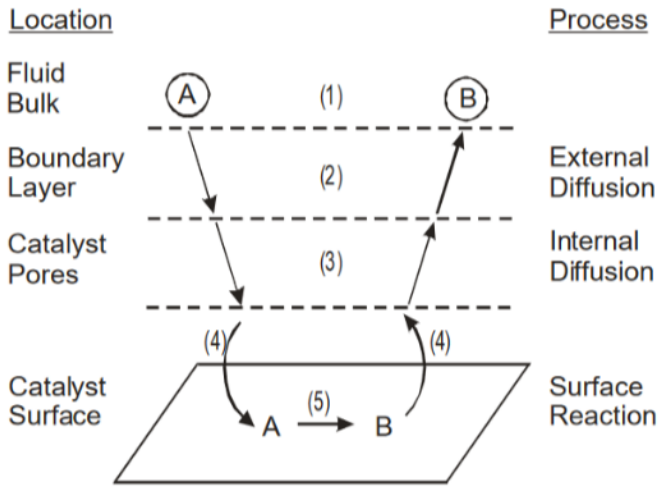

Figure 5: Multi-step process of Diffusion for Reacting Species between Catalyst Surface and Exhaust Gas (Fluid) [27]

The governing equation in GT-Suite to represent the diffusion process are:

Solid phase energy,

$$\psi_s \frac{\partial T_s}{\partial t} = \frac{\partial}{\partial z}\left(f_{sb}\lambda_{sb}\frac{\partial T_s}{\partial z}\right) + hS(T_g - T_S) - \sum_{n=1}^{nrct} \Delta H_n a_n \bar{r_n} + \frac{P}{V} + h_x s_x (T_x - T_s)$$

Gas phase energy,

$$\epsilon \rho_g v C_{pg} \frac{\partial T_g}{\partial z} = |hS(T_s - T_g)$$

Continuity,

$$\frac{\partial}{\partial z}(\rho_g v) = 0$$

Momentum,

$$\epsilon \frac{\partial p}{\partial z} + \frac{\partial v}{\partial z}(\epsilon \rho_g v) = -S_f \frac{1}{2}\rho_g v^2$$

The Nusselt number represents the convective to conductive heat transfer ratio across a fluid boundary [28]. The Nusselt number is used to quantify the enhancement of heat transfer through convection relative to conduction across the same fluid layer.

The heat and mass transfer coefficients can be related to a single Nusselt number in the context of the fully-developed laminar flow down a channel[28].

$$h = Nu\frac{\lambda_g}{D_h}$$

$$k_{m,i} = Sh\frac{\rho_g D_{i,m}}{D_h}$$

Symbol/Variable	**Description**

a_n	active site density of reaction n [mol-site/m^3]
C_{pg}	heat capacity of gas [J/kg K]
D_h	hydraulic diameter of the channel [m]
$D_{i,m}$	binary diffusion coefficient of trace species *i* in the mixture [m^2/s]
f	friction factor
f_{sb}	solid fraction of substrate
h	heat transfer coefficient [J/(m^2 s K)]
h_x	external heat transfer coefficient [J/(m^2 s K)]
$k_{m,i}$	mass transfer coefficient for trace species I [kg/(m^2 s)]
ΔH	Enthalpy of reaction
Nu	Nusselt number for heat transfer
P	power input [J/s]
r_n	reaction rate for reaction n [mol/(mol-site s)]
S	surface area per reactor volume [m^{-1}]
S_x	external surface area per reactor volume [m^{-1}]
Sh	Sherwood number for mass transfer
t	time [s]
T_g	temperature of bulk gas in reactor channels [K]
T_s	temperature of gas at catalyst surface [K]
T_x	external temperature [K]

v	interstitial velocity [m/s]
V	reactor volume [m^3]
z	axial position [m]
ϵ	void fraction of reactor
λ	thermal conductivity of bulk gas [J/(m s K)]
λ_{sb}	thermal conductivity of substrate [J/(m s K)]
ρ_g	density of bulk gas in reactor channels [kg/m^3]
ψ_s	effective heat capacity of reactor [$J/(m^3 K)$]

Table 4:Variable/Symbol Description for Mass and Heat Transfer Equations

Chemical Kinetics

Modeling the catalytic reactions is challenging due to complex reactions and high sensitivity to exhaust gas temperature and emissions species. To implement the chemical reaction over the catalyst substrate, we use the 'SurfaceReaction' template.

The surface reactions that take place in the catalyst bricks are the most crucial part of chemical kinetic modeling. Every chemical reaction has a temperature dependency and the relation between the reaction rate and temperature is represented by the Arrhenius equation. GT-Suite follows the rate expressions for chemical kinetics as mentioned in below,

$$R = A * \exp\left(-\frac{E_A}{RT}\right) * conc * cov * G(i)$$

In the above equation $A, E_a, R, T, conc, cov$ & $G(i)$ represent pre-exponent multiplier, activation energy, universal gas constant $\left(8.314\ \frac{J}{mol-K}\right)$, concentration

expression, coverage expression or coverage fraction, and inhibition function, respectively[29]

The chemical reactions that occur on the surface, specifically for adsorption and desorption, follow either Eley-Rideal or Langmuir Hinshelwood reactions. The Langmuir-Hinshelwood mechanism involves the adsorption of reactant molecules onto a catalyst surface, followed by their reaction to form products. The mechanism assumes that reactant molecules independently adsorb onto vacant surface sites and then react with each other. The adsorbed reactants can either react directly with each other or undergo desorption from the surface before reacting. The Eley-Rideal mechanism describes a different scenario: one reactant is already adsorbed on the catalyst surface, and another reactant collides with the adsorbed species to form products. The incoming reactant collides with the adsorbed species and reacts with it to produce products. The rate reactions for SCR and ASC generally follow the Langmuir-Hinshelwood reaction mechanism[30].

The reactions over the surface of the catalyst are dictated by the availability of catalyst over the washcoat surface. The washcoat has the active catalyst loaded for the exhaust species to react. Hence, the governing relation to obtain the right value to represent the catalyst properties accurately can be determined by the following relation,

The atomic weight is calculated based on $Pt{:}\,Pd$ ratio, and it is determined by the following relationship,

$$At.Wt.\left(\frac{g}{mol}\right) = \frac{x}{x+1}(Pt) + \frac{1}{x+1}(Pd)$$

$x \rightarrow Pt{:}\,Pd$ ratio (E.g., 3:1)

$Pt \rightarrow$ Atomic weight of platinum

$Pd \rightarrow$ Atomic weight of palladium

The active site density (ASD) can be calculated by,

$$ASD = \left(\frac{loading_{site,element}}{At.Wt}\right) * dispersion_{factor}$$

The dispersion factor is the ratio of active site to total sites available on washcoat. This parameter can be used to represent aging, poisoning, etc. The loading represents the density of the catalyst over the washcoat surface.

Solver Theory

The GT-Suite model uses the quasi-steady solver for the standalone ATS models to generate solutions and results. The quasi-steady (QS) solver uses relatively larger time steps to reduce computation time as the exhaust gas flow through the catalyst is at a higher flow rate reducing the residence time within the catalyst. The QS solver computes the thermodynamics of the ATS, and the QS solver discretizes the catalyst volume into sub-volumes. Hence a finer sub-volume would generate smoother temperature prediction curves but takes a heavy toll on the computation time.

To solve the chemical kinetics of the ATS, the solver and its attributes significantly affect the performance of the ATS. GT offers different types of solvers,

- Advanced Adaptive (AA)
- Fixed Mesh (FM)
- Backward Differentiation Formula (BDF)

The AA and FM solvers are recommended for ATS modeling, whereas the BDF solver can be used but is not recommended. The AA solver is designed for reactors with storage components in their catalyst formulations. It employs numerical methods and utilizes a dynamically-adjusting, spatially-non-uniform mesh. The most challenging part of the computation, the species equations, are solved efficiently on this mesh. The solver's adaptive mesh ensures accurate and efficient simulations of reactors by generating mesh at each time step, making it valuable for optimizing such systems [31][32].

The FM solver is robust and uses a fixed axial mesh without the quasi-steady assumption[10], [31]. In contrast, the Advanced Adaptive solver automatically resolves reaction fronts with its adaptive mesh, making it faster. Both solvers can handle adaptive time steps and large master time steps. The FM solver is a slower alternative to the AA solver, requiring discretizing the catalyst into smaller sub volumes for accurate resolutions.

The BDF solver is a numerical integrator designed for stiff Ordinary Differential Equations (ODEs) with both fast and slow dynamics. Unlike the Runge-Kutta method, it avoids needing small time steps and offers better numerical stability. However, this method is computation heavy. The BDF solver efficiently handles stiff systems, especially in models with detailed reaction kinetics and rapid changes. Hence, it is effective for models incorporating fast and slow chemical kinetics and was found to be a robust solver[33].

When the individual catalyst bricks were combined in a single model, the solver for each chemical reaction must be changed from AA or FM to BDF. If the required change is not incorporated, the model runs into solver errors causing the simulation to terminate immediately. Hence, changing the solver to BDF resolves this issue. Moreover, the BDF solver was found to be a robust solver. The exact algorithm for each of the solvers is proprietary to GT-Suite [34].

GT-Suite features an optimization known as the Integrated Design Optimizer (IDO), an inbuilt search tool that help in optimizing different parameters. The IDO is used to find the right parameter value to minimize the error function. The IDO hosts a variety of different searching algorithms. One of the optimization methods is the accelerated genetic algorithm. The accelerated genetic algorithm improvises the results of genetic algorithm using metamodeling[35] . From past studies it has been observed that the accelerated genetic algorithm can provide better solutions within fewer design iterations.

Since the model calibration is done over transient data. The temperatures profiles and the exhaust emission species flow rate were set as transient targeting objects. The optimizer tries to optimize the root mean squared error (RMSE) between each target value and the simulation. In the optimization process, the parameters for temperature predictions were optimized and then the surface reaction parameters were optimized.

$$error = \frac{\sqrt{\int_{t_{start}}^{t_{end}} \left(X(t) - X(t)_{target}\right)^2 dt}}{\sqrt{t_{end} - t_{start}}}$$

$X(t) \rightarrow$ Simulated signal / value

$X(t)_{target}$ → Target signal / value

t_{start} → Simulation start time

t_{end} → Simulation end time

It was observed that GT-Suite had a limitation where at an instance only one emission species can be optimized if the exhaust species concentration is defined in fractions, percentage or parts-per-million (PPM), different terms weights could not be added. Hence instead, the species flow rate was selected as a target to optimize the emission species.

METHODOLOGY

Formulation of the Aftertreatment System Model

The modeling of the ATS is based off the close-packaged ATS architecture. The catalyst layout forms the basis of the modeling of the ATS in GT-Suite.

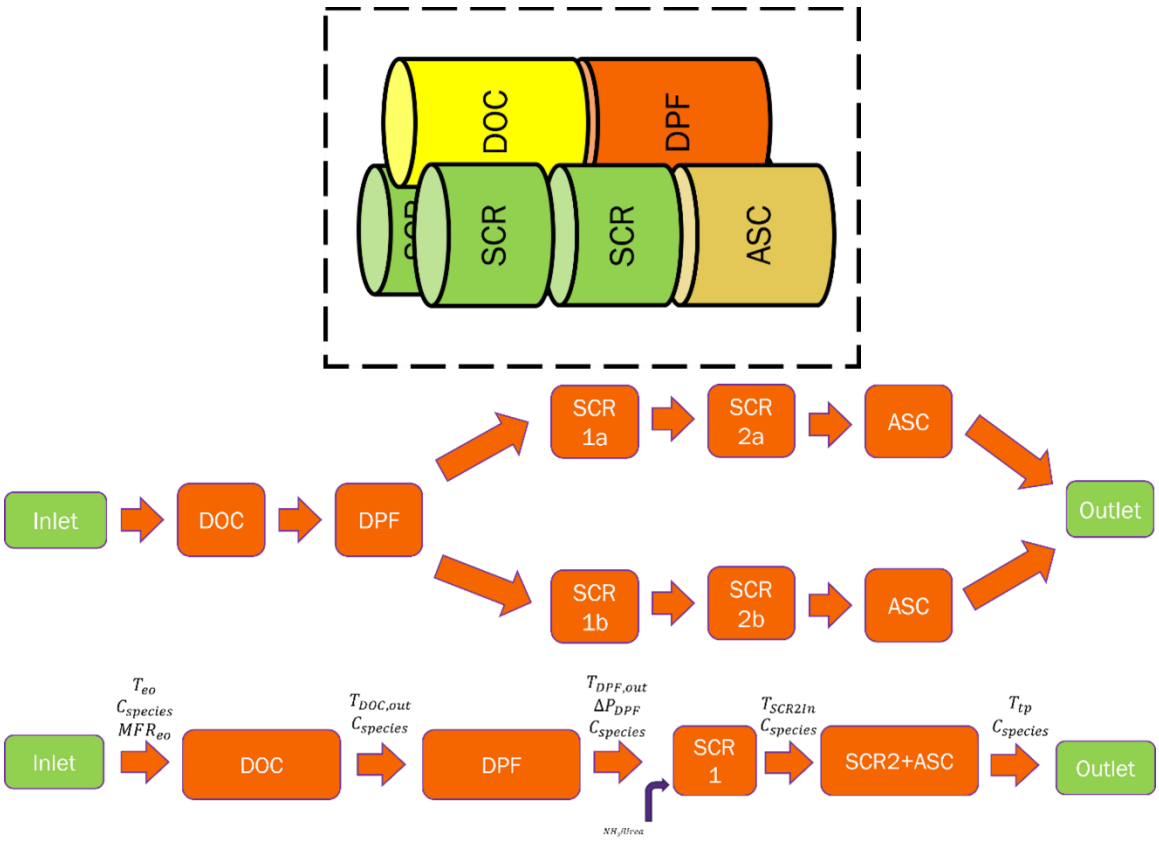

Figure 6: Close-Packaged Aftertreatment System Layout/Schematic

In the modeling of the aftertreatment system in GT-suite, it is essential that the model needs to be robust and predict temperature and emission species over variety of drive cycles. The developed ATS model is calibrated, tested and validated over transient

cycles i.e., cold FTP and hot FTP. The cold FTP and hot FTP are the same drive cycles with identical torque demands and exhaust mass flow rates. The only difference between the two is exhaust gas temperature since the engine operates in different modes as the initial state of the engine and aftertreatment is different.

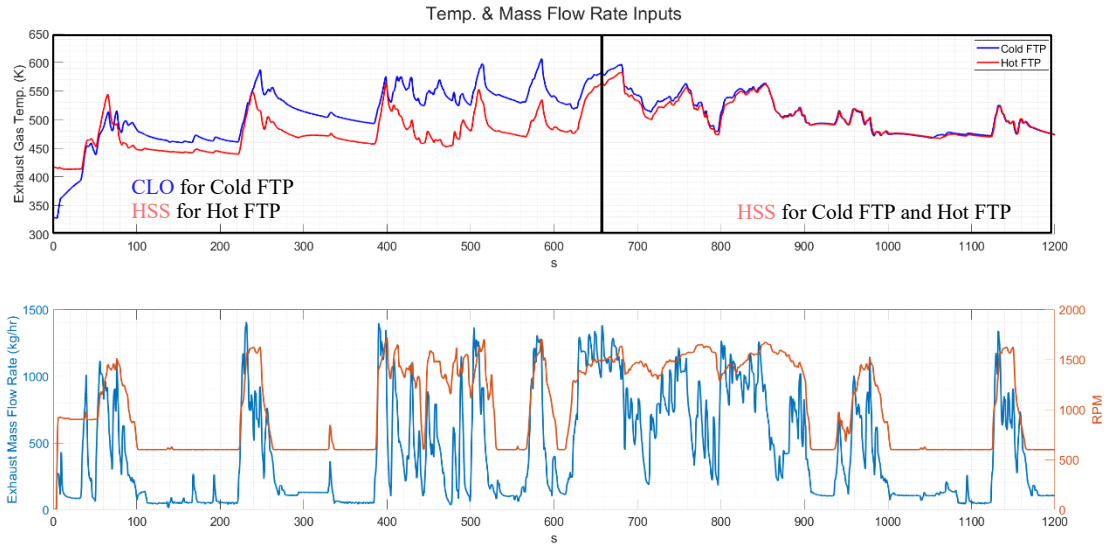

Figure 7: Temperature and Mass Flow Rate Inputs

From the figure 7, it can be observed that the engine operates in two different modes, the Catalyst Light-Off (CLO) and Hot Steady State (HSS). The CLO mode helps in catalyst to reach light-off temperature, the temperature at which the conversion efficiency of the ATS is 50%, and HSS maintains the ATS temperature. We can observe that the cold FTP has higher exhaust gas temperature and energy which allows to warm up the ATS components. Once the ATS reaches the light-off temperature, the engine mode switches to keep the ATS at an optimal temperature.

The system's behavior is highly dictated by the temperatures, the reactions follow the principles for the Arrhenius equation. Hence, there are a variety of calibration parameters within the GT-model.

The modeling approach for the project was divided into multiple steps,

Step1: Identifying the system inputs

Based on the availability of the experimental data, the inputs that were necessary for the standalone ATS model were, exhaust mass flow rates, temperatures of the exhaust gas, concentration of exhaust gas species $CO, NO, NO_2, CO_2, O_2, C_3H_6$ (HCs), H_2O and soot. For the SCRs, concentration of NH_3 was introduced to the model through mass flow rate of diesel exhaust fluid [DEF].

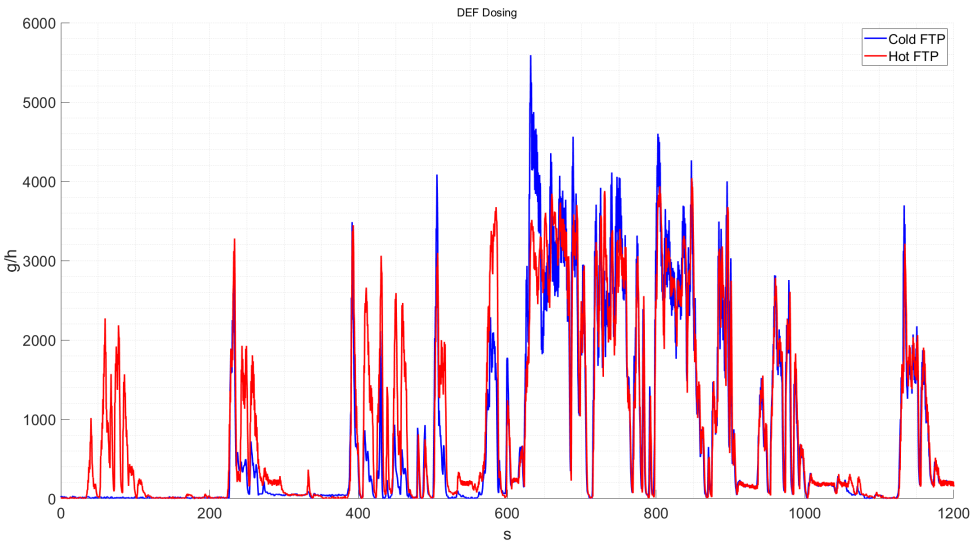

Figure 8: Mass Flow Rate of DEF Dosing

The available concentration of HCs was in C1 basis, hence the concentration was modified in such a manner that the all the HCs fed to the model were in C3 basis. The

reason to feed the model with C3 HCs was that the reactions associated with C_3H_6 are classified as fast reactions.

Step2: Integration of independent catalyst

The models which are independently developed are integrated into a single model to represent the Close-packaged ATS. In this stage the intermediate connections are also integrated and modeled as which includes the pipes and other volumes within the ATS. The models' thermal properties were calibrated or calculated by assuming a large chamber with dimensions close to the actual ATS.

Step3: Optimization of the parameters

Once the integration of all the bricks was completed an optimizer was run to get the optimum values for the physical parameters of the bricks that would be suitable for accurate prediction of the temperature. The temperature predictions of the GT-Suite model were validated through the temperature and pressure sensors that were located before and after the DOC, DPF and the SCR/AMOX chamber. The schematic of the sensor's locations is specified in Figure 9.

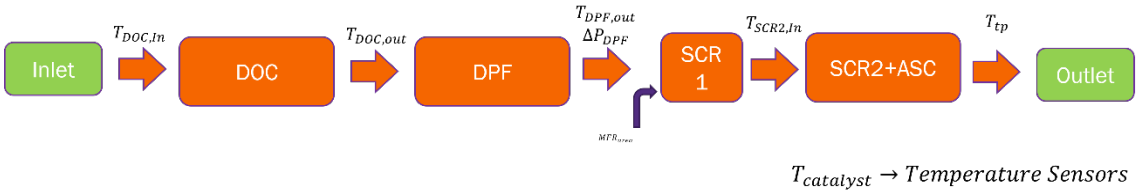

Figure 9: Sensor Location Schematic

Once the optimized values for the physical parameters of the catalyst bricks were obtained the model was updated with the values. The optimizer was able to give an insight on the sensitivity analysis of the parameters and the dependency of the target profiles on the parameters that required to be optimized.

Calibration Process

The calibration process can be well understood from the figure below,

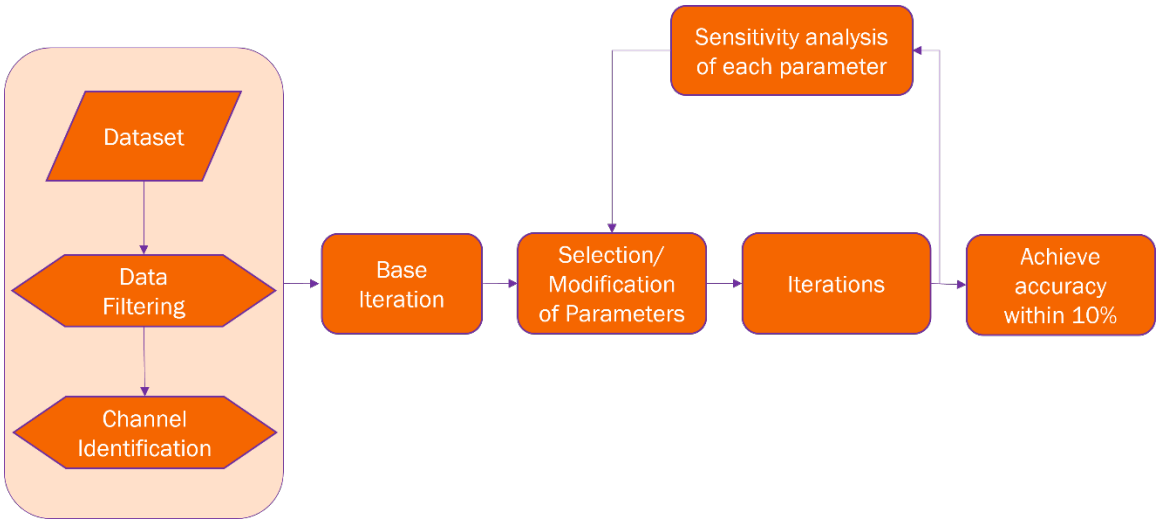

Figure 10: Process for Model Calibration

The dataset available here is the transient data, which is recorder over the cold FTP and hot FTP drive cycles. The data is captured at a frequency of 2Hz and did not have noise, and seemed post-processed, hence data filtration was not done. The channels for the inputs were identified. The channels for the exhaust mass flow rate, temperature from the thermocouples, and pressure drop channels were available. For emissions species, FTIR measurement channels were referred for engine out and tailpipe species concentration. However, for NO_x data from the NO_x sensors were referred for engine out and tailpipe concentrations.

Inlet Conditions

Once the right data is channels are identified, the model was fed with the following input conditions:

a. Mass flow rate of the exhaust gas

b. Exhaust gas temperature at ATS inlet

c. Species concentration in parts-per-million (PPM)

d. Mass flow rate of soot

e. Mass flow rate of DEF

To simplify the model, NH_3 was directly induced into the exhaust stream. The following relation was used to calculate the conversion/correction factor for DEF mass flow rate,

Conversion/Correction factor:

$$NH_{3_{FlowRate}} = K_{NH_3} * DEF_{FlowRate}$$

$$K_{NH_3} = \left(x \frac{mol}{s}\ NO_x\right)\left(\frac{1\ mol\ NH_3}{1\ mol\ NO_x}\right)\left(\frac{1\ mol\ urea}{2\ mol\ NH_3}\right)\left(\frac{60g\ urea}{1\ mol\ urea}\right)\left(\frac{1g\ solution}{0.325g\ urea}\right)$$

$$K_{NH_3} = \frac{1}{\left(\frac{92.317}{17.031}\right)}$$

$$K_{NH_3} = \frac{1}{5.42}$$

$$NH_{3_{FlowRate}} = 0.18 * \mathrm{DEF}_{FlowRate}\ \left[\frac{g}{hr}\right]$$

Physical Specifications and Chemical Kinetics Specifications

The geometric specifications of the catalyst brick were incorporated within the GT-Suite model as per the given specifications. The 1D model of the ATS, uses the 'CatalystBrick' template to represent each catalyst component within the Close-packaged

ATS. The template has two most important sections, the main section where all the geometric specifications are added, and the thermal section to define attributes that will represent the thermal properties of the catalyst brick.

For the reactions surface reaction kinetics, there can be various chemical reaction mechanisms that we can choose to represent the actual chemical kinetics of the catalyst surface. Hence, GT-Suite allows us to model these reactions using 'SurfaceReaction' template which allows us to specify attributes that govern the chemical reactions. The specific attributes are defined and explained further for each catalyst. For modeling the washcoat thickness is assumed to be 10% of the substrate thickness.

The geometric specifications of each component are:

	Size (inches)	**Cells-per-sq. inch (CPSI)**	**Total Substrate Thickness $mil(thou)$**
DOC	ϕxx $*$ y	xx	xx
DPF	ϕxx $*$ y	xx	xx
SCR1	ϕxx $*$ y	xx	xx
SCR2	ϕxx $*$ y	xx	xx
ASC	ϕxx $*$ y	xx	xx

Table 5: Catalyst Brick Specification

The catalyst specifications/description are:

Specification/Description for Catalysts	
DOC	xx
DPF	xx
SCR1	xx
SCR2	xx
SCR3	xx

Table 6: Catalyst Specification/Description

Casing

The casing of the Close-packaged is an essential component for convective heat transfer. The casing is modeled in a way such that convective the heat transfer takes place between the catalyst and the walls of the casing and not ambient temperature, such that the sink temperature is the temperature of the casing. The heat transfer of the casing takes place between the casing's outer layer and ambient. This allows us to have very low convective heat transfer coefficient for the catalyst components to retain the thermal mass gained from the exhaust gas. Another way to model this is by calculating an average external heat transfer coefficient for each component including the casing and imposing that over other ATS components.

Diesel Oxidation Catalyst

On the basis of the description from Table 6, the DOC is split into two volumes with same geometric specification, except the length. The DOC is split into two sub volumes, in order to have different chemical kinetics for the DOC. Although the key reactions and inhibition functions are same, the active site densities are different.

The reactions kinetics are adapted from previous studies conducted for cold start applications for DOC [36]. The reactions were modified to consider only the fast

reactions for hydrocarbons, over C3 basis so to avoid more calibration parameters for slow reactions for diesel vapors. The past studies have considered and simulated similar systems to represent fast chemical kinetics for propylene [37].

	DOC Vol. 1	**DOC Vol. 2**
Loading of Site Element (g/ft^3)	xx	xx
Atomic Weight (g/mol)	xx	xx
Dispersion Factor	0.05	0.05

Table 7: Active Site Density Calculation Parameters for DOC

Site Element	**Reactants**	**Products**	**Pre-exponent multiplier**	**Activation Energy or Temperature (J/mol or K)**	**Concentration expression**
PGM	$2CO + O_2$	$2CO_2$	1.18E+12	81330	$\{CO\} * \{O_2\}/(G(1) * G(2))$
PGM	$2C_3H_6 + 9O_2$	$6CO_2 + 6H_2O$	1.57E+19	159400	$\{C_3H_6\} * \{O_2\}/(G(1) * G(2))$
PGM	$2H_2 + O_2$	$2H_2O$	98300	15310	$\{H_2\} * \{O_2\}/(G(1) * G(2))$
PGM	$2NO + O_2$	$2NO_2$	1327	6721	$1 * (\{NO\} * \sqrt{(\{O_2\})} - \{NO_2\} * G(4)/G(5))/(G(3) * G(2))$

Table 8: Governing Reaction Equations for DOC

$\boldsymbol{G(i)}$	Description	General and Inhibition Function
1	CO inhibition	$(1.0 + 248.* exp(-614.9/T) * \{CO\})\text{^}2$
2	NO inhibition	$1 * (1.0 + 0.242 * exp(4861./T) * \{NO\})$
3	Hydrocarbon inhibition	$(1.0 + 2.02e - 17 * exp(2.823e4/T) * (\{C_3H_6\}))\text{^}2$
4	Conversion factor from NO oxidation Keq to Kc, units $(mole/m^3)^{0.5}$	$sqrt(101325/8.314/T)$
5	NO oxidation equilibrium constant Keq	$1.5E - 4 * exp(6864/T)$

Table 9: Governing General and Inhibition Functions for DOC

Diesel Particulate Filter

The model for DPF has passive regeneration, hence the catalyst specifications for the catalyzed substrate for DPF was modeled for the surface reactions. The loading is assumed to be for both active sites for surface reactions, as well as the soot packaging density for the substrate, for DPF filter properties[19], [38], [39].

	DPF
Loading of Site Element (g/ft^3)	xx
Atomic Weight (g/mol)	xx
Dispersion Factor	0.3

Table 10: Active Site Density Calculation Parameters for DPF

Site Element	**Reactants**	**Products**	**Pre-exponent multiplier**	**Activation Energy or Temperature (J/mol or K)**	**Concentration expression**
c-NASA(soot)	$C + NO_2$	$CO + NO$	1E7	12000	$\{NO_2\} * G(1)$
c-NASA(soot)	$C + 2\,NO_2$	$CO_2 + 2\,NO$	1E7	12000	$\{NO_2\} * G(2)$
c-NASA(soot)	$C + 0.5O_2$	CO	1E8	24000	$\{O_2\} * G(3)$
c-NASA(soot)	$C + O_2$	CO_2	1E8	24000	$\{O_2\} * G(4)$

Table 11: Governing Reactions Equations for DPF Regeneration

$\boldsymbol{G(i)}$	Description	General and Inhibition Function
1	selectivity factor for CO for passive regen	0.9
2	selectivity factor for CO2 for passive regen	0.1
3	selectivity factor for CO for active regen	0.1
4	selectivity factor for CO2 for active regen	0.9

5	Conversion factor from NO oxidation Keq to Kc, units (mole/m^3)^0.5	$sqrt(101325/8.314/T)$
6	NO oxidation equilibrium constant Keq	$1.5E-4*exp(6864/T)$

Table 12: Governing General and Inhibition Functions for DPF

Selective Catalyst Reduction

The SCR is the most complex portion of the modeling piece, since we have two sets of SCR with two SCR of same kind in a set. The first set of SCRs, i.e. SCR1 and SCR2 are split into sub volumes, to model it similar to how the DOC is modeled. The SCR is split into sub volumes based on the length and catalyst type only since the loading and active site density was unknown. The model uses chemical kinetics for dual layer catalyst, where the active sites are copper chabazite (Cu-CHA) and iron zeolite (Fe-Z) as it closely represents the catalyst chemical activity specifications for the first set of the SCRs. The second set of SCRs have only one catalyst loading over the washcoat, hence a similar catalyst chemical activity mechanism for copper chabazite (Cu-CHA) is used.

The model has dual layers for Fe-Z of the same kind, the second layer assists in maximizing the adsorption and desorption efficiency of NH_3 over the catalyst surface to improve the SCR performance.

Various studies have used other catalysts and compared the performance, that have vanadium, titanium oxide, etc. [22], [40]. The dual layer catalysts have better performance due to higher catalyst density over the washcoat. The reaction mechanisms for SCRs have storage modeled for NH_3 over the washcoat to improvise the performance[11], [41], [42].

Site Element	Reactants	Products	Pre-exponent multiplier	Activation Energy or Temperature (J/mol or K)	Concentration expression
Cu-CHA	$NH_3 + S$	SNH_3	665	0	$\{NH_3\}$
Cu-CHA	SNH_3	$NH_3 + S$	1.00E+12	0	$G(1)$
Cu-CHA	$2SNH_3 + 1.5O_2$	$N_2 + 3H_2O + 2S$	2.00E+12	22100	$\{O_2\}$
Cu-CHA	$NO + 0.5O_2$	NO_2	190	6655	$\{NO\} * \{O_2\}\text{^}0.5 - \{NO_2\} * G(2)/G(3)$
Cu-CHA	$4SNH_3 + 4NO + O_2$	$4N_2 + 6H_2O + 4S$	2.50E+09	11330	$\{NO\}$
Cu-CHA	$2SNH_3 + NO + NO_2$	$2N_2 + 3H_2O + 2S$	5.10E+12	10500	$\{NO\} * \{NO_2\}$
Cu-CHA	$4SNH_3 + 3NO_2$	$3.5N_2 + 6H_2O + 4S$	7.00E+12	17000	$\{NO_2\}$
Cu-CHA	$2SNH_3 + 2NO_2$	$N_2 + SAN + H_2O + S$	8100	5780	$\{NO_2\}$
Cu-CHA	SAN	$N_2O + 2H_2O + S$	4460	5600	1
Fe-Z1	$NH_3 + FeZ1$	$FeZ1NH_3$	54.6	0	$\{NH_3\}$
Fe-Z1	$FeZ1NH_3$	$NH_3 + FeZ1$	3.00E+08	0	$G(4)$
Fe-Z1	$2FeZ1NH_3 + 1.5O_2$	$N_2 + 3H_2O + 2FeZ1$	10000	11530	$\{O_2\}$
Fe-Z1	$NO + 0.5O_2$	NO_2	5.44	3210	$\{NO\} * \{O_2\}\text{^}0.5 - \{NO_2\} * G(5)/G(6)$
Fe-Z1	$4FeZ1NH_3 + 4NO + O_2$	$4N_2 + 6H_2O + 4FeZ1$	2140000	9090	$\{NO\}/G(7)$
Fe-Z1	$2FeZ1NH_3 + NO + NO_2$	$2N_2 + 3H_2O + 2FeZ1$	1.16E+13	9630	$\{NO\} * \{NO_2\}$
Fe-Z1	$4FeZ1NH_3 + 3NO2$	$3.5N_2 + 6H_2O + 4FeZ1$	3.00E+12	17490	$\{NO_2\}$
Fe-Z1	$2FeZ1NH_3 + 2NO_2$	$N_2 + FeZ1AN + H_2O + FeZ1$	18000	5420	$\{NO_2\}$
Fe-Z1	$FeZ1AN$	$N_2O + 2H_2O + FeZ1$	50000	5060	1
Fe-Z1	$2N_2O$	$2N_2 + O_2$	6.40E+07	16000	$\{N_2O\}$
Fe-Z1	$2FeZ1NH_3 + 3N_2O$	$4N_2 + 3H_2O + 2FeZ1$	2350000	11440	$\{N_2O\}$
Fe-Z2	$NH_3 + FeZ2$	$FeZ2NH_3$	1.6	0	$\{NH_3\}$
Fe-Z2	$FeZ2NH_3$	$NH_3 + FeZ2$	1.80E+08	0	$G(8)$

Table 13: Governing Equations Reactions for SCRs

$G(i)$	Description	General and Inhibition Function
1	Desorption coverage dependent activation energy	$exp(-145900/8.314/T * (1 - 0.97 * A(SNH_3)))$
2	Conversion factor from NO oxidation Keq to Kc for units mole fraction, (P/Po)^-0.5	$sqrt(101325/8.314/T)$
3	NO oxidation equilibrium constant K_{eq}	$1.5E-4 * exp(6864/T)$
4	S1 Desorption Activation Term	$exp(-145900/8.314/T * (1 - 0.97 * A(FeZ1NH_3)))$
5	Conversion factor from NO oxidation K_{eq} to Kc, units (mole/m^3)^0.5	$sqrt(101325/8.314/T)$
6	NO Oxidation Equilibrium Constant	$1.5E-4 * exp(6864/T)$
7	NH3 Inhibition for Standard SCR Reaction	$1 + (1e6)/(4.5e12)/exp(-115000/8.314/T * (1 - 0.45 * A(FeZ2NH_3))) * \{NH_3\} * 8.314 * T/P$
8	S2 Desorption Activation Term	$exp(-115000/8.314/T * (1 - 0.45 * A(FeZ2NH_3)))$

Table 14: Governing General and Inhibition Functions for SCRs

Ammonia Slip Catalyst

The ammonia slip catalyst has a similar layout to the SCRs. There are total two ASC parallel to each other and downstream of the SCRs. The Ammonia slip catalyst unlike the SCR does not have any storage modeled. This is to comply with the reaction mechanisms [43], [44] that are used for modeling the chemical kinetics.

	ASC
Loading of Site Element (g/ft^3)	xx
Atomic Weight (g/mol)	xx
Dispersion Factor	0.05

Table 15: Active Site Density Calculation Parameters for ASC

Site Element	Reactants	Products	Pre-exponent multiplier	Activation Energy or Temperature (J/mol or K)	Concentration expression
Pt	$2NH_3 + 1.5O_2$	$N_2 + 3H_2O$	2.27E+18	19000	$\{NH_3\} * \{O_2\}/G(1)$

Pt	$2NH_3 + 2.5O_2$	$2NO + 3H_2O$	3.20E+25	27200	$\{NH_3\} * \{O_2\}/G(1)$
Pt	$2NH_3 + 2NO + 1.5O_2$	$2N_2O + 3H_2O$	4.52E+20	18210	$\{NH_3\} * \{NO\} * \{O_2\}/G(1)$
Pt	$NO + 0.5O_2$	NO_2	1.12E+07	5250	$(\{NO\} * sqrt(\{O_2\}) - \{NO_2\} * G(2)/G(3))/G(1)$
Pt	$2NH_3 + 2NO_2$	$N_2 + N_2O + 3H_2O$	6.27E+13	6530	$\{NH_3\} * \{NO_2\}$
Pt	$2NH_3 + 1.5O_2$	$N_2 + 3H_2O$	2.27E+18	19000	$\{NH_3\} * \{O_2\}/G(1)$
Pt	$2NH_3 + 2.5O_2$	$2NO + 3H_2O$	3.20E+25	27200	$\{NH_3\} * \{O_2\}/G(1)$

Table 16: Governing Reaction Equations for ASC

$G(i)$	**Description**	**General and Inhibition Function**
1	NO2 inhibition	$1.0 + 3.3E6 * exp(-1330/T) * \{NO_2\}$
2	Conversion factor from NO oxidation Keq to Kc, units (mole/m^3)^0.5	$sqrt(101325/8.314/T)$
3	NO oxidation equilibrium constant Keq	$1.5E-4 * exp(6864/T)$

Table 17: Governing General and Inhibition Functions for ASC

GT-Suite Layout

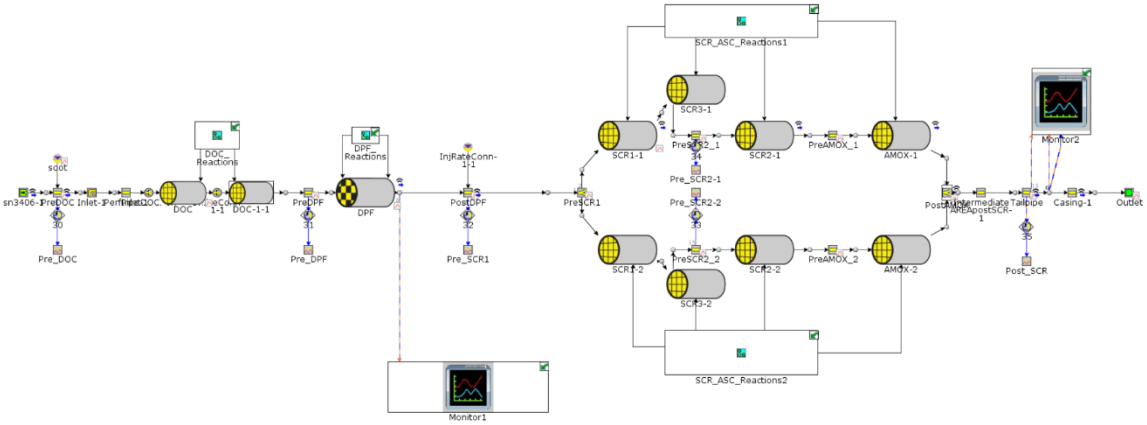

Figure 11: GT-Suite Aftertreatment System

Thermal Optimization

The optimization process for the model to accurately predict temperature takes into account the parameters that affect the thermal inertia and the heat transfer properties of the system. Since the only known parameters for the catalyst bricks were the frontal diameter, length, substrate thickness and washcoat thickness. The remaining parameters about the catalyst were unknown and hence they are used as tuning parameters to accurately match the temperatures from the experimental data.

The following parameters are varied:

Parameter	**Range of Optimization**
Casing wall thickness	2mm – 10mm
Casing external convective heat transfer coefficient	$5\ \frac{W}{m^2-K} - 20\ \frac{W}{m^2-K}$
Casing surface emissivity	0.1 – 1
Pipe external convective heat transfer coefficient	$5\ \frac{W}{m^2-K} - 20\ \frac{W}{m^2-K}$

Pipe wall thickness	2mm – 10mm
Pipe surface emissivity	0.1 – 1
DOC outer layer thickness	2mm – 10mm
DOC outer layer emissivity	0.1 – 1
DOC external convective heat transfer	$0.001\ \frac{W}{m^2-K}$ – $20\ \frac{W}{m^2-K}$
DPF outer layer thickness	2mm – 10mm
DPF outer layer emissivity	0.1 – 1
DPF external convective heat transfer	$0.001\ \frac{W}{m^2-K}$ – $20\ \frac{W}{m^2-K}$
Substrate Pore Diameter (DPF)	10 microns – 40 microns
Substrate Porosity (DPF)	0.4 – 0.6
SCR outer layer thickness	2mm – 10mm
SCR outer layer emissivity	0.1 – 1
SCR external convective heat transfer	$0.001\ \frac{W}{m^2-K}$ – $20\ \frac{W}{m^2-K}$
ASC outer layer thickness	2mm – 10mm
ASC outer layer emissivity	0.1 – 1
ASC external convective heat transfer	$0.001\ \frac{W}{m^2-K}$ – $20\ \frac{W}{m^2-K}$

Table 18: Parameters for Thermal Calibration

Chemical Kinetic Optimization

The optimization for the chemical kinetics is driven by the reaction rates. Hence, the optimizer is set for the pre-exponent multiplier and the activation energy for the reactions that take place in the DOC and the second set of the SCRs. Ideally for calibration techniques like TPR and TPD are used[17], [45].

These techniques are commonly used in catalysis studies to characterize and optimize the performance of SCR catalysts. Previous studies review different transient methods that can be used for determining reaction kinetics. Transient methods allow extracting more information about the reaction kinetics than steady-state methods. Although both the methods can be used for to characterize the catalysts, but TPR is

suitable as a transient kinetic tool to understand chemical and physical behavior of the catalyst[46], [47].

The results obtained from the first set of the SCRs proved to have a higher NO conversion percentage. Hence, the parameters that are tuned are mentioned.

Parameter	**Range for Optimization**
Dispersion Factor (DOC)	5 % - 35 %
Dispersion Factor (DPF)	5 % - 35 %
Active Site Density (SCR1)	10 mol/m^3 – 1000 mol/m^3
Active Site Density (SCR2)	10 mol/m^3 – 1000 mol/m^3
Dispersion Factor (ASC)	5 % - 35 %

Table 19: Parameters for Chemical Kinetic Calibration

DOC

Reactions	**Range for Optimization**	
	Pre-exponent multiplier	**Activation Energy (J/mol)**
$CO + 0.5O_2 \rightarrow CO_2$	$10^{10} - 10^{14}$	75000 – 86000
$C_3H_6 + 4.5O_2 \rightarrow 3CO_2 + 3H_2O$	$10^{17} - 10^{21}$	130000 – 180000
$H2 + 0.5O_2 \rightarrow 2H_2O$	$10^{2} - 10^{6}$	13000 – 17000
$NO + 0.5O_2 \rightarrow NO_2$	$10^{2} - 10^{5}$	8000 – 12000

Table 20: Parameters for Chemical Kinetic Calibration for DOC

SCR

Reactions	**Range for Optimization**	
	Pre-exponent multiplier	**Activation Temperature (K)**
$NO + 0.5O_2 \rightarrow NO_2$	$10^{0} - 10^{4}$	4000 – 8000
$4SNH_3 + 4NO + O_2 \rightarrow 4N_2 + 6H_2O + 4S$	$10^{6} - 10^{10}$	8000 – 13000
$2SNH_3 + NO + NO_2 \rightarrow 2N_2 + 3H_2O + 2S$	$10^{10} - 10^{14}$	8000 – 13000
$4SNH_3 + 3NO_2 \rightarrow 3.5N_2 + 6H_2O + 4S$	$10^{10} - 10^{14}$	15000 – 19000
$2SNH_3 + 2NO_2 \rightarrow N_2 + SAN + H_2O + S$	$10^{1} - 10^{5}$	3000 – 7000

Table 21: Parameters for Chemical Kinetic Calibration for SCR

ASC

Reactions	**Range for Optimization**	
	Pre-exponent multiplier	**Activation Temperature (K)**
$2NH3 + 1.5O2 \rightarrow N2 + 3H2O$	$10^{16} - 10^{20}$	17000 – 21000
$2NH3 + 2.5O2 \rightarrow 2NO + 3H2O$	$10^{23} - 10^{27}$	25000 – 29000
$2NH3 + 2NO + 1.5O2 \rightarrow 2N2O + 3H2O$	$10^{18} - 10^{22}$	16000 – 20000
$NO + 0.5O2 \rightarrow NO2$	$10^{5} - 10^{9}$	3000 – 7000
$2NH_3 + 2NO_2 \rightarrow N_2 + N_2O + 3H_2O$	$10^{11} - 10^{15}$	4000 – 8000

Table 22: Parameters for Chemical Kinetic Calibration for ASC

RESULTS AND DISCUSSION

The results that are obtained for the temperature are for the cold FTP and hot FTP are discussed. The results for the temperature are validated and compared over the experimental data set which includes thermocouple temperature measured downstream of the DOC, DPF and the SCR. The pressure drop across the DPF was also essential part that was calibrated and validated.

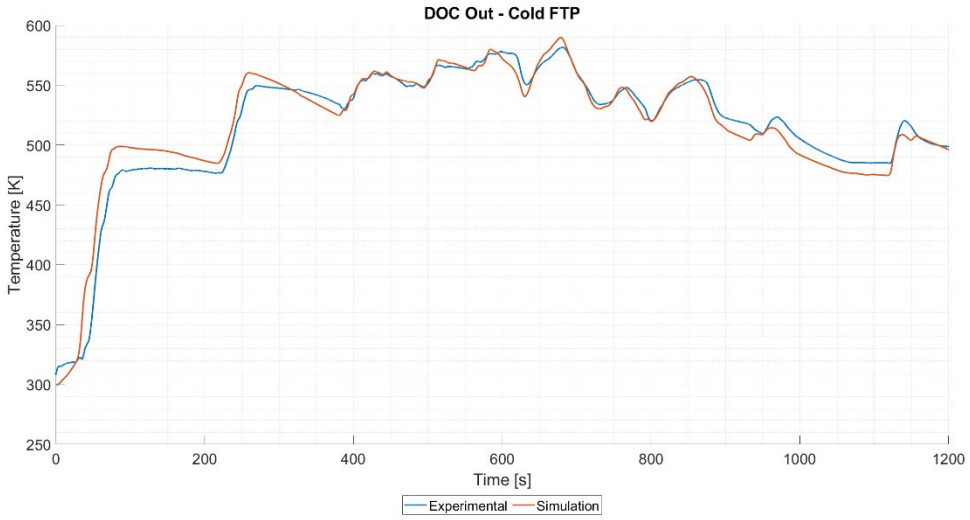

Figure 12: Temperature at DOC Outlet for Cold FTP

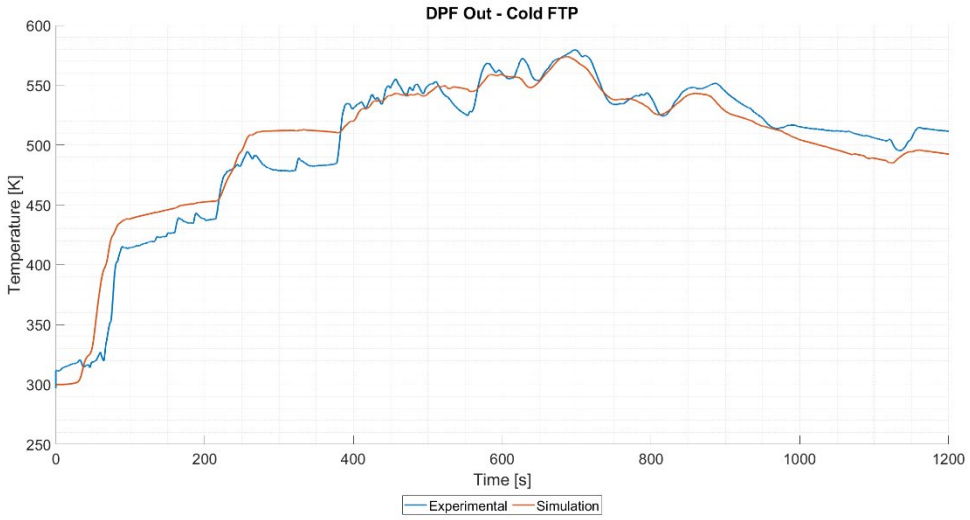

Figure 13: Temperature at DPF Outlet for Hot FTP

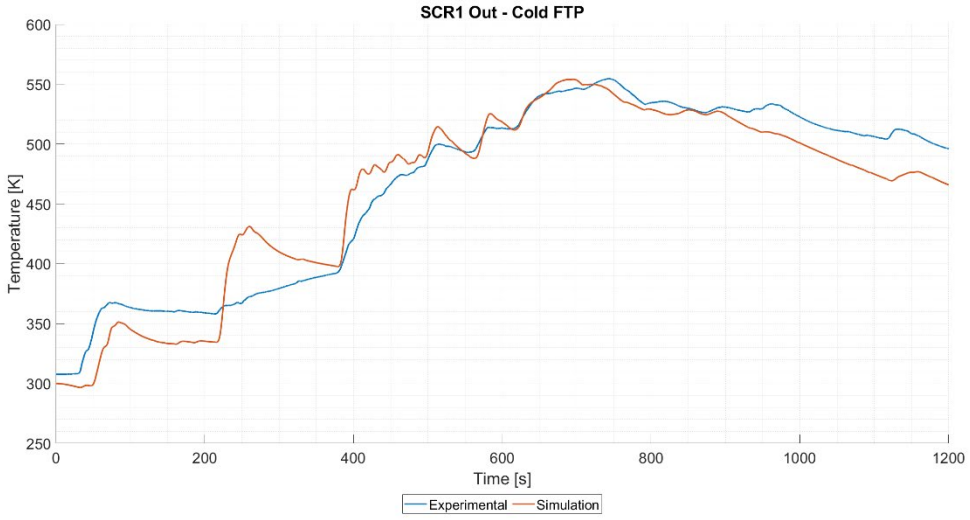

Figure 14: Temperature at SCR1 Outlet for Cold FTP

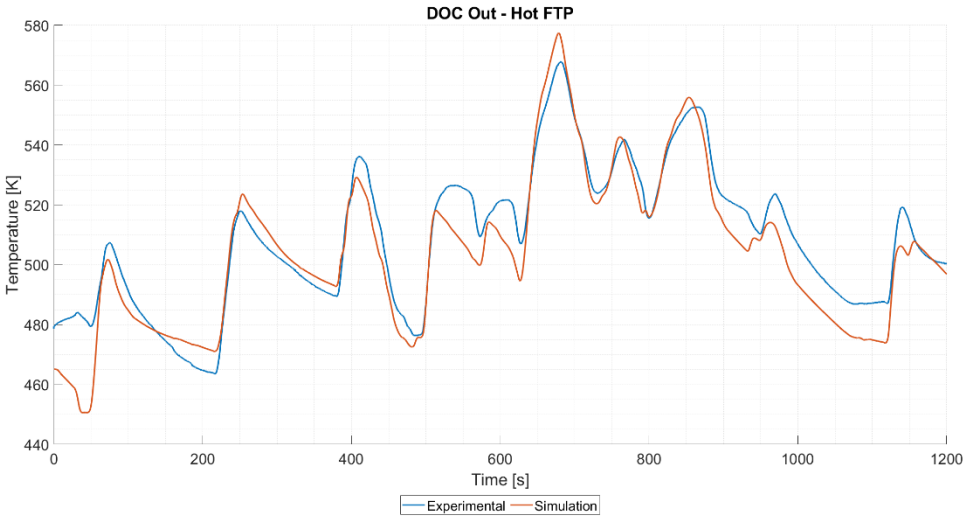

Figure 15: Temperature at DOC Outlet for Hot FTP

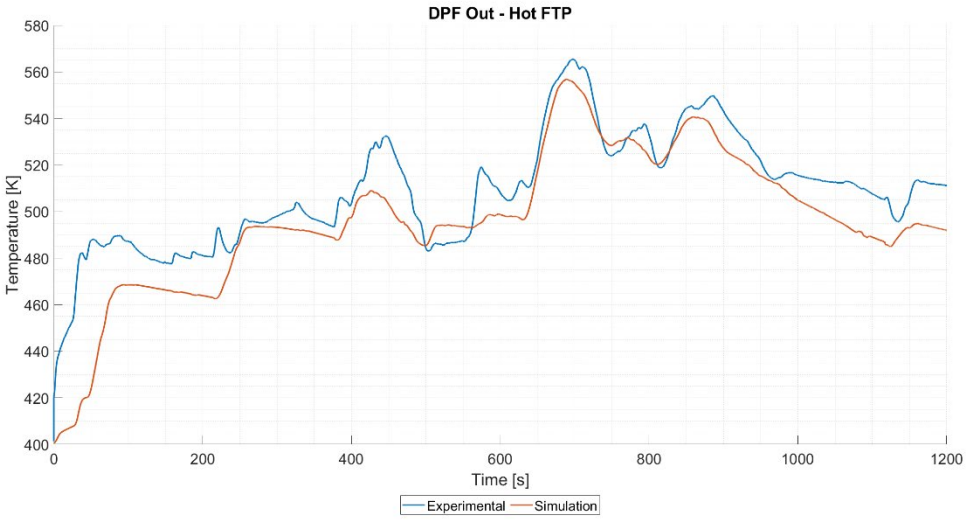

Figure 16: Temperature at DPF Outlet for Hot FTP

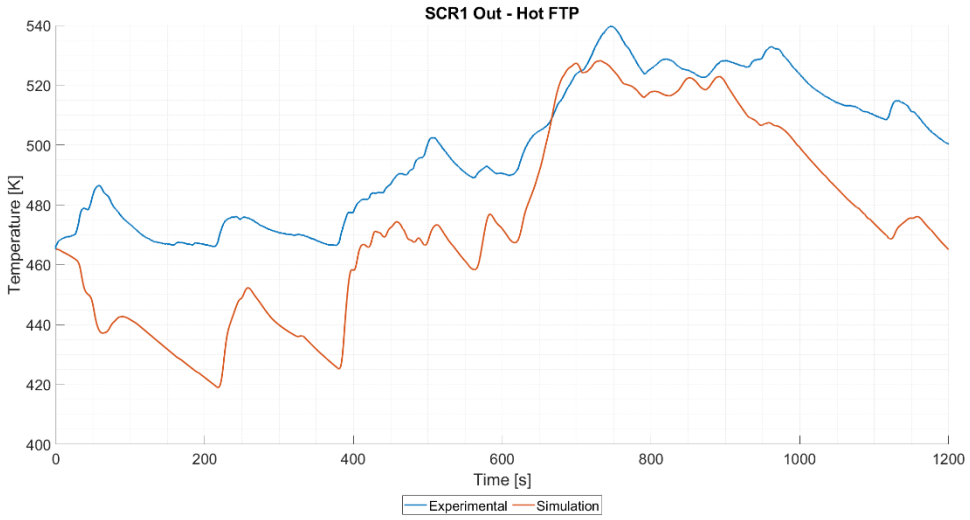

Figure 17: Temperature at SCR1 Outlet for Hot FTP

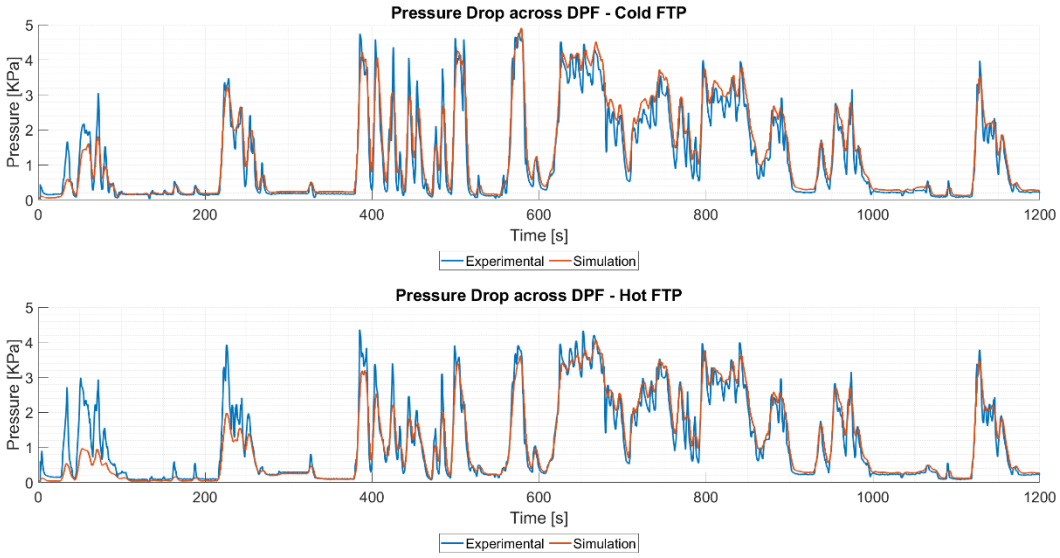

Figure 18: Pressure Drop across DPF for Cold FTP and Hot FTP

The results on the temperature predictions can be improved by having a better fit for the external heat transfer coefficient and heat capacity for the catalyst as well as species. Since the thermal properties of the materials are pre-defined within GT-Suite, hence the material parameters were not modified or optimized within acceptable range.

Once the error is incurred, as the exhaust gas traverse downstream of the ATS, the error with temperatures cascades and increases the overall error. We observe maximum temperature difference for the SCR, since it is densely packaged and is not modeled highly accurately. The pressure difference that is observed is due to the unknown initial soot deposition in the DPF, hence we observe the error in the pressure drop across the DPF. Since the project is still on-going these findings prove to be a good source to learn more about the ATS characteristics.

The ATS model is highly complex and has a very high thermal inertia, the model results can also be improved if the flow within the Close-packaged can be modelled accurately. The flow could not be modeled accurately due to limited information about the system. The potential area of improvement lies in modeling the sub volumes between the DPF, SCR and the tailpipe. The model geometry and volume changes continuously and drastically after the DPF, which affects the temperature of the exhaust gas. The exhaust gas energy might also decrease since it is exposed to other components before it enters the SCRs. Another observation is that we are feeding the model with temperatures captured by the thermocouples, which induces thermocouple delays. Whereas the actual gas temperature would vary when compared to the thermocouples.

In the plot below we can see the difference between the exhaust gas and the thermocouple model, which was added in GT-Suite as per the actual thermocouple specifications.

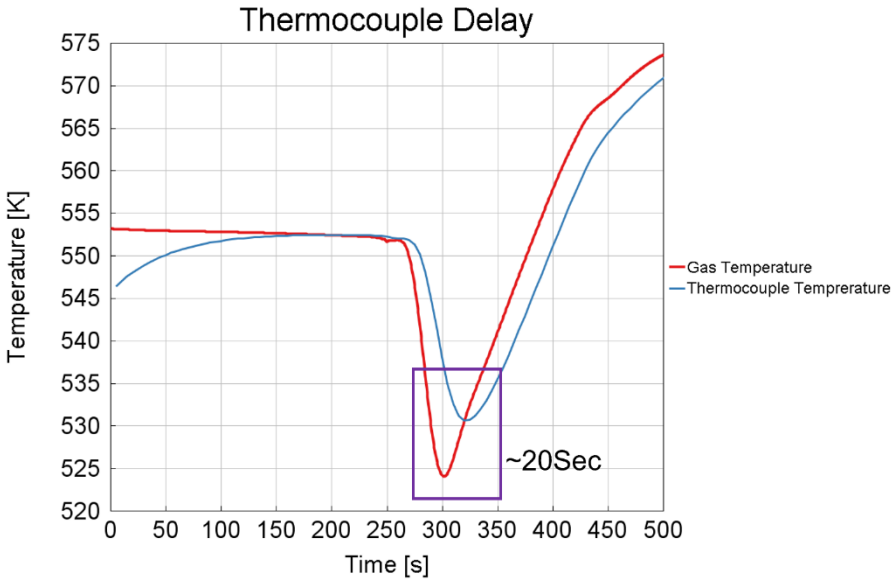

Figure 19: Thermocouple Delay

The model accuracy can be improved when the model is calibrated over steady-state data, as we can model the system to reach a steady state temperature. Based on the time it takes to reach steady-state temperature we can modify the parameters that vary the thermal inertia of each component. This will also allow us to understand the ATS in a better fashion.

The temperature predictions is a major driving factor for the ATS model and developing accurate models for the ATS. As we can observe that a slight change in temperature can affect the performance and the conversion efficiency of the ATS. But with insufficient information for the ATS, to predict the species concentration and accurately predict the behavior of chemical kinetics, the optimizations of the chemical kinetics parameters were necessary.

Based of the model results, to validate the ATS conversion efficiency maps were generated and validated against the past research.

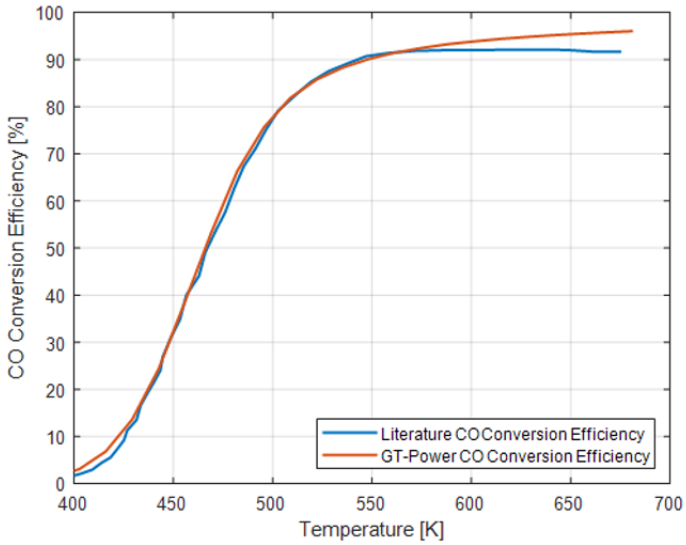

Figure 20: CO Conversion Efficiency[48]

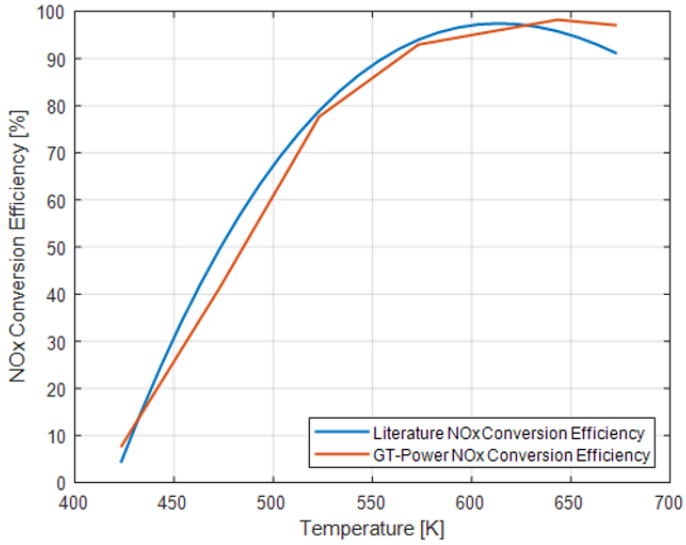

Figure 21: NO_x Conversion Efficiency[49]

For this project predicting CO and NO_x emissions were a high priority, the model results can be observed below.

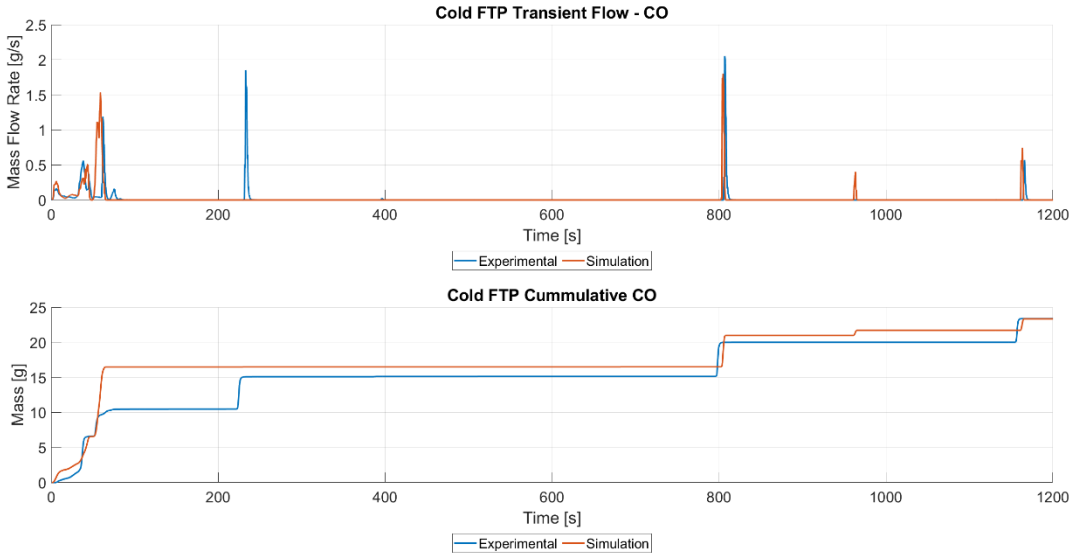

Figure 22: Transient and Cumulative CO Flow Rate for Cold FTP

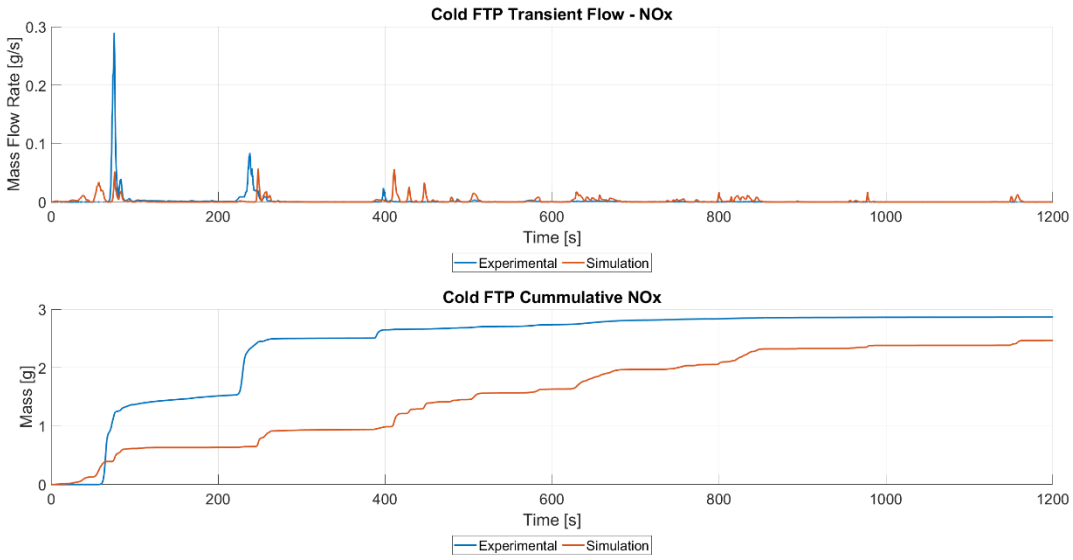

Figure 23: Transient and Cumulative NO_x Flow Rate for Cold FTP

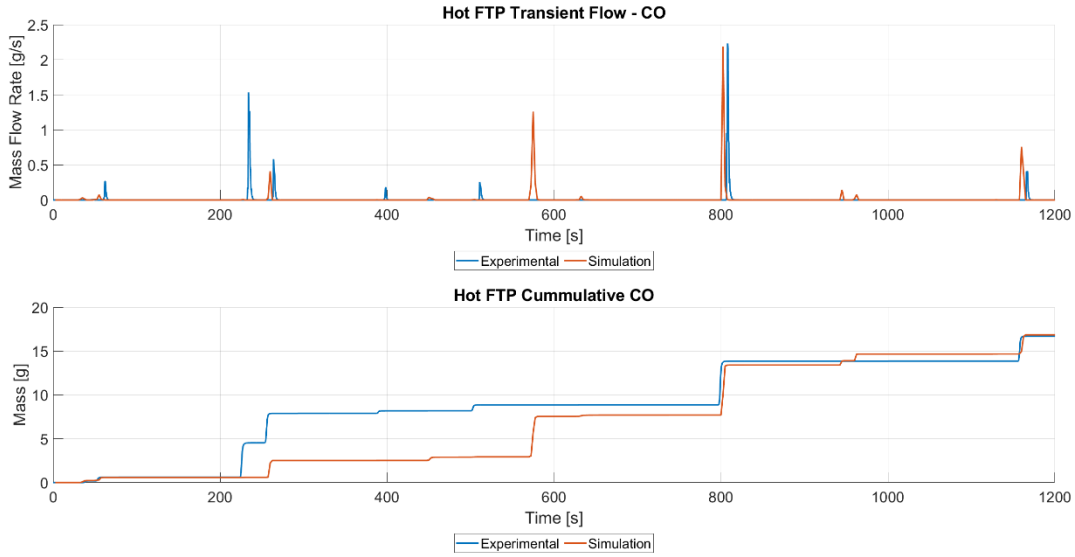

Figure 24: Transient and Cumulative CO Flow Rate for Hot FTP

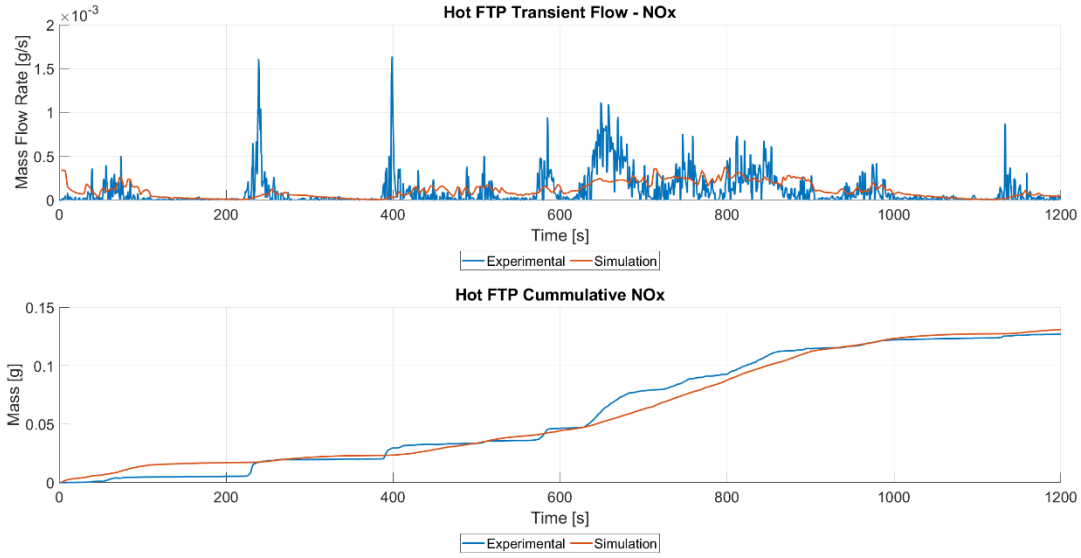

Figure 25: Transient and Cumulative NO_x Flow Rate for Hot FTP

The model is fairly accurate when we consider the cumulative predictions made by the model for CO and NO_x concentrations. The model has cumulative error, NO_x and CO combined, of 9.8% and 1% for cold FTP and hot FTP respectively. We observe that

the model seems to capture the transients but tends to skip or miss out on the spike that we observe near 200s. This is a consistent trend which we observe in both cold FTP and hot FTP. This is specifically observed in CO flow rate. For NO_x flow rate the cold FTP has a magnitude error in the first 150s, but later follows the drive cycle closely. The initial error in NO_x concentration contributes to the overall error in concentration prediction.

To explore the reasons for the error, the data and the results were analyzed to eliminate possible sources for error. The areas of error are:

a. Engine Operation

   The engine operation plays a vital role. The spikes that the simulation misses and causes error to occur after engine idle periods and when there is rapid variation in engine speed. These trends are observed in CO, HC and soot as well as the engine operates rich or, at a lower air-fuel ratio. This reduces the oxygen concentration which causes deficiency during oxidation.

b. Inconsistent calibration data set

   The actual system is exposed to higher exhaust gas temperatures/energy which may not be captured or be observed form the experimental data. The model does include storage only for NH_3 and not other species, it is assumed that the exhaust gas species is not trapped in and is a perfect exchanger, which is unlike the actual system.

c. Active site densities

The active sites were calibrated by the optimizer hence it is difficult to represent the actual system. The model aging can be accounted by a certain extent, sub volume aging would be tough to model and drastically affect the simulation run times.

The model parameters were varied to observe the system behavior closely. The simulation was conducted over the cold FTP as the low temperature behavior can be understood and characterized correctly. The optimization parameters were varied in multiple iterations. It was observed that in some cases we can accurately track the transient behavior for CO and in some cases we can track the transient behavior for NO_x. This is observed in the Figure 24.

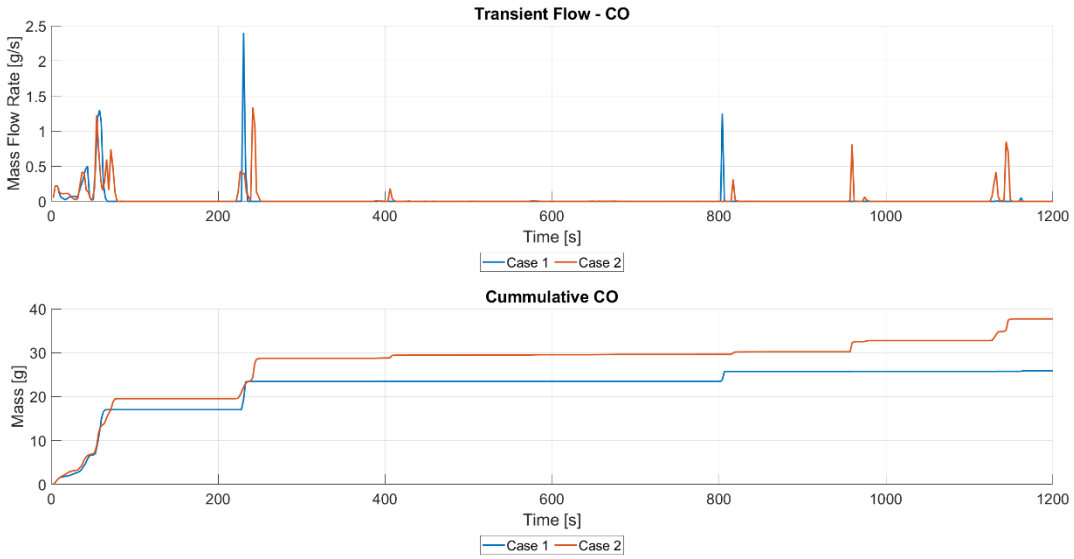

Figure 26: Transient and Cumulative CO for Cold FTP under varied parameters

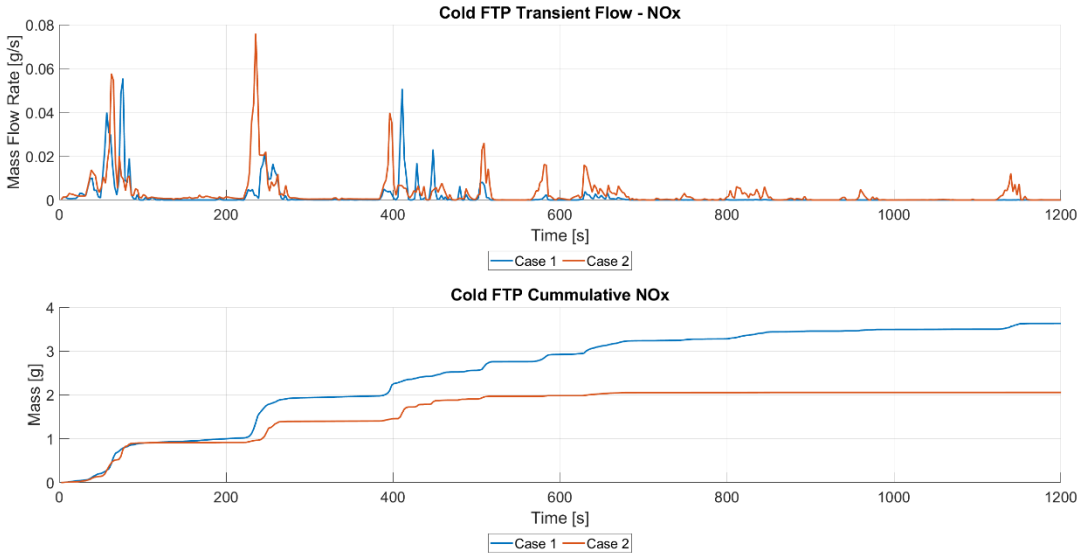

Figure 27: Transient and Cumulative NO_x for Cold FTP under varied parameters

The active sites have the highest priority, since we the active sites represent the availability for the chemical to react and the reaction rate are calculated based on the active site available at a time step. So, in rapid transient that model can have the sites saturated and the catalyst activity can have an upper limit as per the available sites. Hence, the active sites may saturate and have limited conversion of the exhaust species based on the rate reaction priority which is guided by the activation temperature or energy[50].

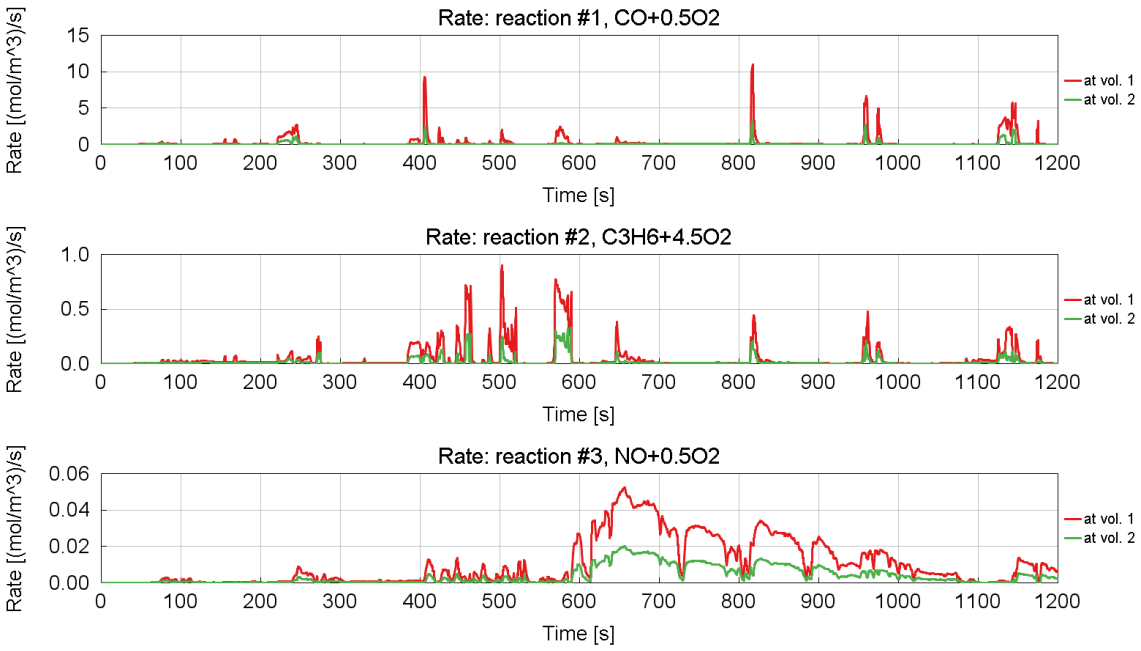

Figure 28: Reaction Rates of Reactions in DOC for Cold FTP

The reaction rate plots from the DOC depicts the activity of the catalyst to basically identify the regions where the CO spikes that exists and the saturation of the active sites is reached at that time step. These behaviors characterize the unavailability of the active sites to cause any sort of species conversion.

The model's accuracy can be improved by calibrating reaction rates at low temperatures and specifically for cold FTP cycle as it the tailpipe emission generation is high when compared to hot FTP. The temperature and pressure drop calibration can directly affect the 1D simulation results which indirectly affect the reaction rates and emissions concentrations. The discrepancy while validation can be eliminated by accurate experimental measurements. The GT-Suite model can predict better results but will take a toll on the simulation runtimes.

To better understand the results the ATS is run over multiple steady state operating points for two different engine operation modes. The catalyst lights off (CLO) and the hot steady state (HSS). The difference between the two modes have been discusses earlier.

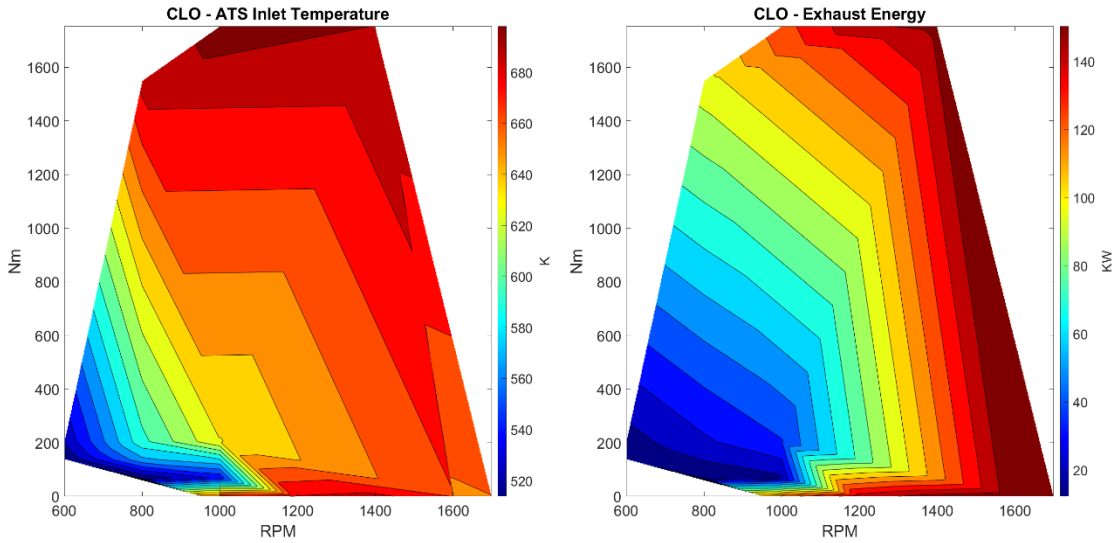

Figure 29: Exhaust Gas Temperature and Energy for Catalyst-Light-off Mode

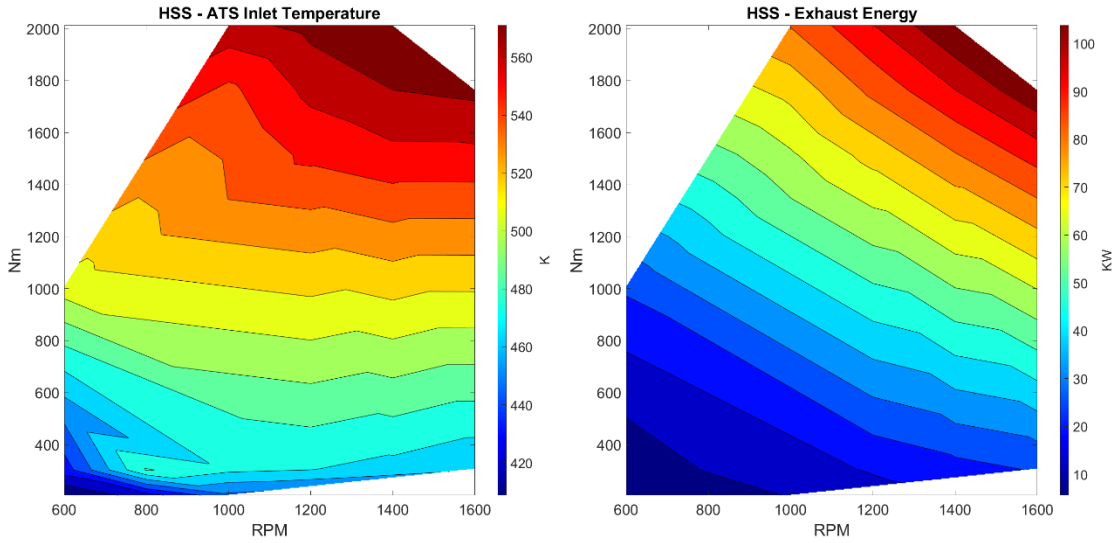

Figure 30: Exhaust Gas Temperature and Energy for Hot-Steady-State Mode

The model was also set to run over steady-state data to support and understand the importance for the calibration purpose and to also develop strategies for heavy-duty hybrid powertrain control. The validity of the ATS over the steady state data cannot be quantified, as the tailpipe data was unavailable during the time of research. But the steady state data gives us important highlights brick temperatures, conversion efficiency and tailpipe emissions concentrations.

The steady state data trends can be observed below for two engine operation modes, the CLO and HSS. Based on the two modes the ATS was fed with relevant inputs and the behavior is analyzed. The steady state data gives us an insight of the variation in ATS behavior and performance at different engine operating points. The results below specifically compare behavior of the ATS, when the engine is operating at different conditions at fixed engine speed i.e., 1200RPM.

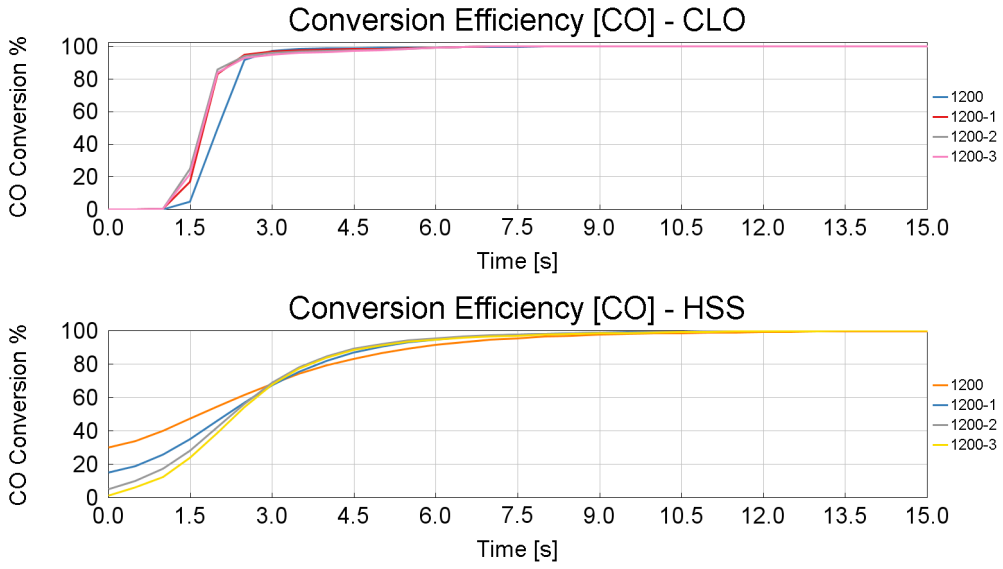

Figure 31: Conversion Efficiency of CO for Catalyst-Light-Off and Hot-Steady-State Mode at fixed RPM (1200-x) with varied engine operating conditions

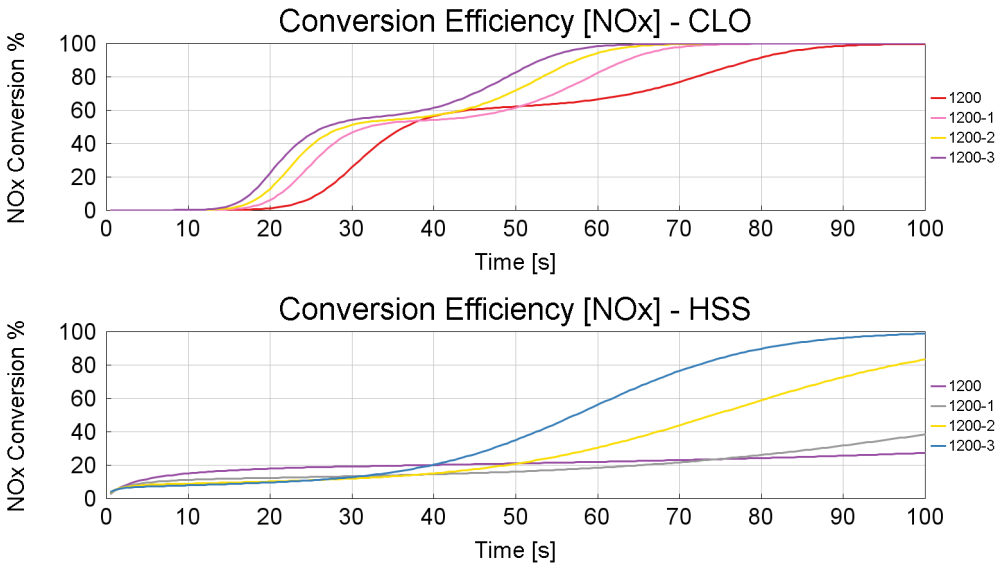

Figure 32: Conversion Efficiency of NO_x for Catalyst-Light-Off and Hot-Steady-State Mode at fixed RPM (1200-x) with varied engine operating conditions

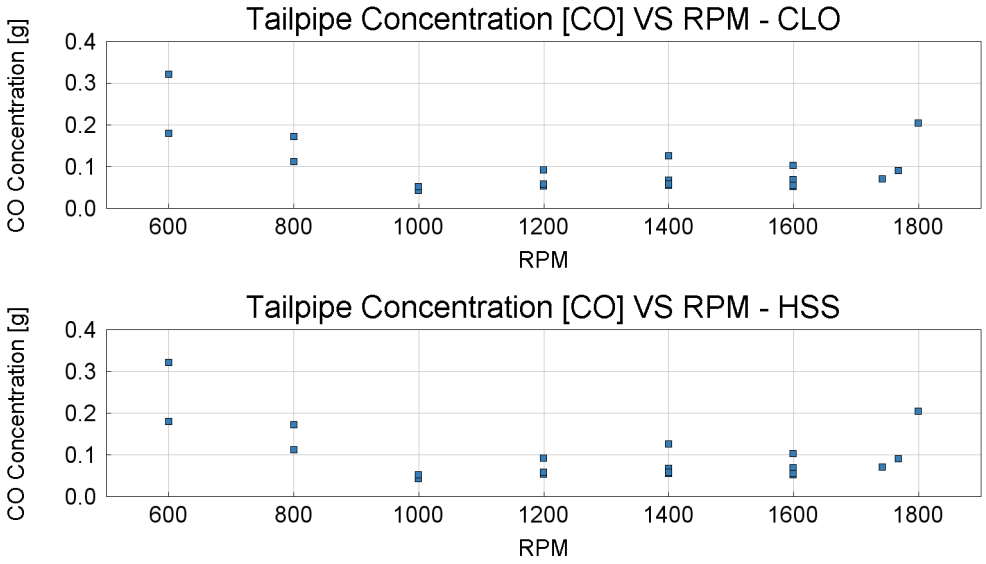

Figure 33: Tailpipe Concentration of CO for Catalyst-Light-Off and Hot-Steady-State Mode

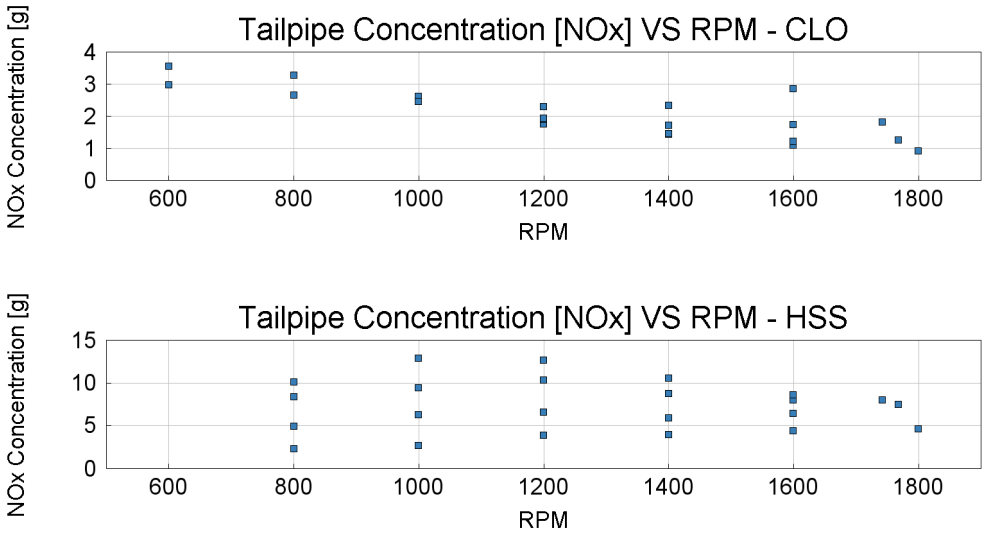

Figure 34: Tailpipe Concentration of NO_x for Catalyst-Light-Off and Hot-Steady-State Mode

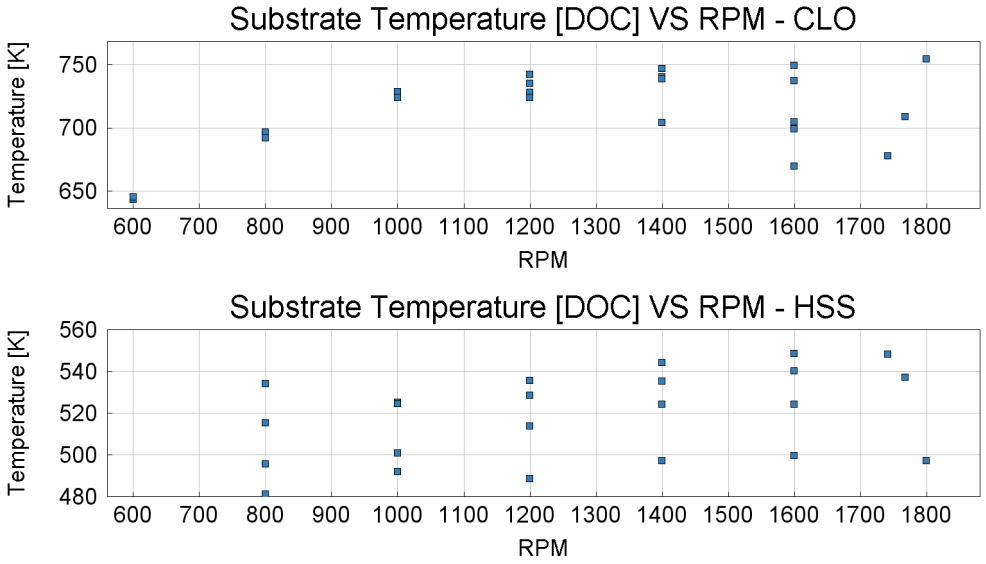

Figure 35: Substrate Temperature of SCR for Catalyst-Light-Off and Hot-Steady-State Mode

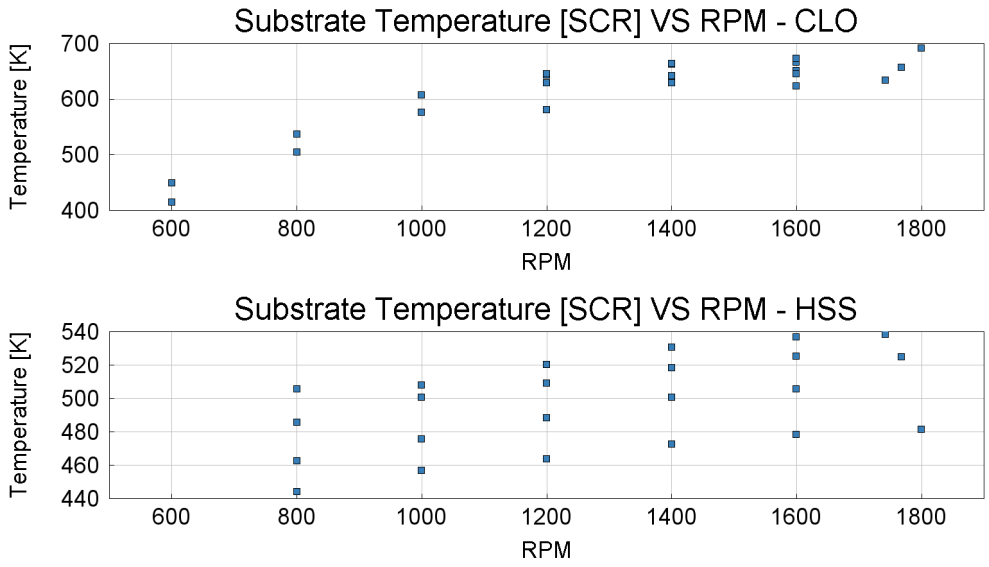

Figure 36: Substrate Temperature of SCR for Catalyst-Light-Off and Hot-Steady-State Mode

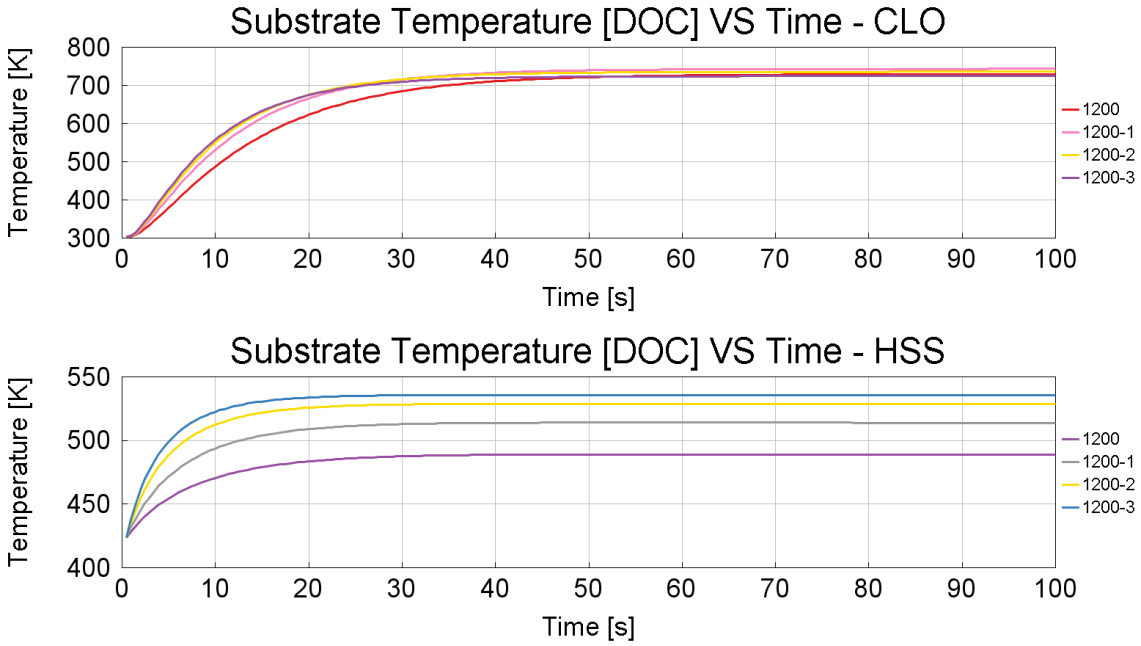

Figure 37: Substrate Temperature of DOC v/s Time for Catalyst-Light-Off and Hot-Steady-State Mode at fixed RPM (1200-x) with varied engine operating conditions

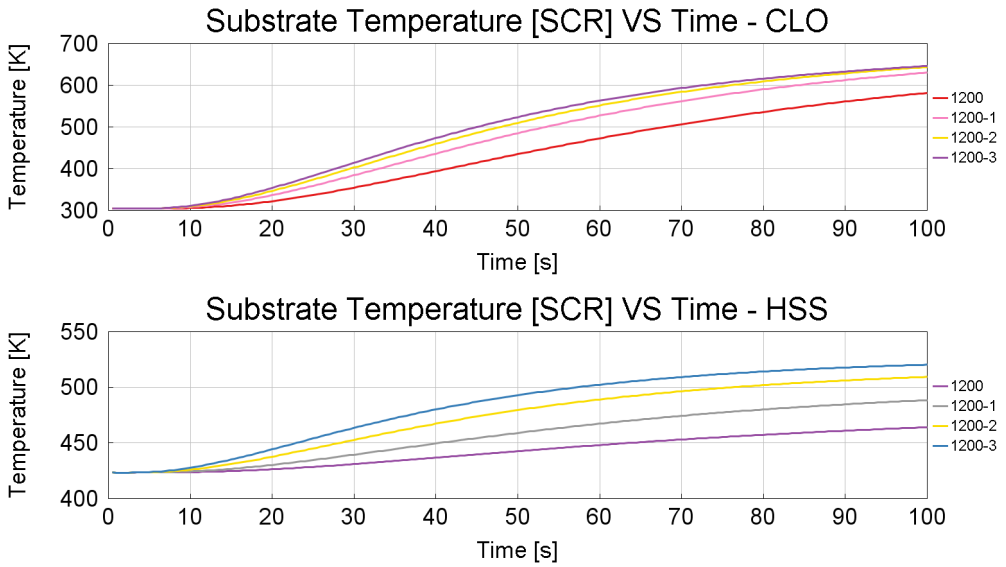

Figure 38: Substrate Temperature of DOC v/s Time for Catalyst-Light-Off and Hot-Steady-State Mode at fixed RPM (1200-x) with varied engine operating conditions

The steady state results allow us to observe the performance of the ATS if run at same engine speeds. The model results can be compared and used to generate maps that will be essential to track different characteristics of the ATS and assist with further research and modeling effort.

CONCLUSION

The goal of this work was to model and evaluate a high-fidelity fast running model of an aftertreatment systems (ATS) in GT-Suite. The models for the DOC, DPF, SCRs and ASC were developed, integrated, calibrated, and evaluated over transient drive cycles. Following are the conclusions of this research study,

- Model run time is ten times faster than real-time, significantly reducing simulation time.
- Calibration process based solely on transient experimental data, speeding up the process but sacrificing some accuracy.
- Temperature calibration involves considering layer thickness, surface emissivity, and external convective heat transfer.
- Temperature gradient inside the catalysts ignored, catalyst bricks treated as a single volume with no discretization.
- Chemical kinetic calibration involves optimizing pre-exponent multiplier, activation energy, and active site density (ASD).
- ASD has the largest impact on ATS performance.
- Model parameters optimized using an accelerated genetic algorithm for improved results.
- Optimization over transients may not be the most reliable due to the root mean square error minimization.

- Species calibration with low tailpipe concentrations may yield less optimal results in the optimization process.
- Steady-state data is highly encouraged for chemical reaction or emission species calibration.
- Model can track temperatures closely and predict exhaust gas concentrations with ~10% accuracy and minimal runtime.
- 1D models may not achieve 100% accuracy without an accurate system model.
- Identified limitations and errors within GT-Suite, providing opportunities for software improvement.
- Ongoing work with the potential for further learning, development, and generation of essential data.

FUTURE WORK

The model developed can be expanded further to accurate represent the Close-packaged ATS in the latest versions of GT-Suite that have better capability to model the ATS dynamics. The model's fidelity can be increased by adding the aging model that can represent catalyst activity axially. To tackle the modeling portion of the ATS, 3D modeling of the ATS can help in accurately characterize the flow inside the Close-packaged ATS and a combination of 3D flow simulations and 1D chemical kinetics can improve the ATS model and would be a good area for research to understand the shortcomings.

The model can be used to generate steady state maps for the ATS temperature, Conversion efficiency, species concentration and thermal behavior of each catalyst to develop supervisory control strategies for hybrid heavy-duty vehicles.

Another domain to explore would include adaptation of the model to comply with hydrogen internal combustion engine emissions. The hydrogen Ice might not require an oxidizing catalyst (DOC) but will require a reduction catalyst for NOx emissions. Although the hydrogen ICE will be significantly compact and reduced but will have a significant impact on tailpipe emissions.

REFERENCES

[1] "Sources of Greenhouse Gas Emissions", [Online]. Available: https://www.epa.gov/ghgemissions/sources-greenhouse-gas-emissions

[2] "Emissions of Carbon Dioxide in the Transportation Sector", [Online]. Available: https://www.cbo.gov/publication/58861

[3] "GHG Distribution", [Online]. Available: https://www.epa.gov/greenvehicles/fast-facts-transportation-greenhouse-gas-emissions

[4] "Control of Air Pollution from New Motor Vehicles: Heavy-Duty Engine and Vehicle Standards." https://www.federalregister.gov/documents/2023/01/24/2022-27957/control-of-air-pollution-from-new-motor-vehicles-heavy-duty-engine-and-vehicle-standards

[5] "40 CFR Part 1036 Subpart E", [Online]. Available: https://www.ecfr.gov/current/title-40/chapter-I/subchapter-U/part-1036/subpart-E

[6] "Proposed Rule: Greenhouse Gas Emissions Standards for Heavy-Duty Vehicles – Phase 3", [Online]. Available: https://www.epa.gov/regulations-emissions-vehicles-and-engines/proposed-rule-greenhouse-gas-emissions-standards-heavy

[7] C. Air Resources Bpard - Mobile Source Control Division, "Appendix I: Current and Advanced Emission Control Strategies and Key Findings of CARB/SwRI Demonstration Work," 2020.

[8] J. B. Heywood, *Internal combustion engine fundamentals*. New York : McGraw-Hill, [1988] ©1988. [Online]. Available: https://search.library.wisc.edu/catalog/999610484402121

[9] Y. Pan, X. Shen, L. Yao, A. Bentalib, and Z. Peng, "Active sites in heterogeneous catalytic reaction on metal and metal oxide: Theory and practice," *Catalysts*, vol. 8, no. 10. MDPI, Oct. 20, 2018. doi: 10.3390/catal8100478.

[10] E. J. Bissett, "An Asymptotic Solution for Washcoat Pore Diffusion in Catalytic Monoliths," *Emission Control Science and Technology*, vol. 1, no. 1, pp. 3–16, Jan. 2015, doi: 10.1007/s40825-015-0010-2.

[11] P. S. Metkar, M. P. Harold, and V. Balakotaiah, "Selective catalytic reduction of NO x on combined Fe- and Cu-zeolite monolithic catalysts: Sequential and dual layer configurations," *Appl Catal B*, vol. 111–112, pp. 67–80, Jan. 2012, doi: 10.1016/j.apcatb.2011.09.019.

[12] S. Dey and G. C. Dhal, "A Review of Synthesis, Structure and Applications in Hopcalite Catalysts for Carbon Monoxide Oxidation," *Aerosol Science and Engineering*, vol. 3, no. 4, pp. 97–131, 2019, doi: 10.1007/s41810-019-00046-1.

[13] W. Addy Majewski, "Selective Catalytic Reduction." https://dieselnet.com/tech/cat_scr.php

[14] P. Peng, X. H. Gao, Z. F. Yan, and S. Mintova, "Diffusion and catalyst efficiency in hierarchical zeolite catalysts," *National Science Review*, vol. 7, no. 11. Oxford University Press, pp. 1726–1742, Nov. 01, 2020. doi: 10.1093/nsr/nwaa184.

[15] S. Govender and H. B. Friedrich, "Monoliths: A review of the basics, preparation methods and their relevance to oxidation," *Catalysts*, vol. 7, no. 2. MDPI, Feb. 16, 2017. doi: 10.3390/catal7020062.

[16] M. Khosravi, A. Abedi, R. E. Hayes, W. S. Epling, and M. Votsmeier, "Kinetic modelling of Pt and Pt: Pd diesel oxidation catalysts," *Appl Catal B*, vol. 154–155, pp. 16–26, 2014, doi: 10.1016/j.apcatb.2014.02.001.
[17] D. Chatterjee, T. Burkhardt, M. Weibel, I. Nova, A. Grossale, and E. Tronconi, "SP-2140)," 2007.
[18] Z. Zhang, R. Dong, G. Lan, T. Yuan, and D. Tan, "Diesel particulate filter regeneration mechanism of modern automobile engines and methods of reducing PM emissions: a review," *Environmental Science and Pollution Research*, vol. 30, no. 14. Springer Science and Business Media Deutschland GmbH, pp. 39338–39376, Mar. 01, 2023. doi: 10.1007/s11356-023-25579-4.
[19] C. Görsmann, "Catalytic coatings for active and passive diesel particulate filter regeneration," *Monatshefte fur Chemie*, vol. 136, no. 1. pp. 91–105, Jan. 2005. doi: 10.1007/s00706-004-0261-z.
[20] R. Dong, Z. Zhang, Y. Ye, H. Huang, and C. Cao, "Review of Particle Filters for Internal Combustion Engines," *Processes*, vol. 10, no. 5. MDPI, May 01, 2022. doi: 10.3390/pr10050993.
[21] P. Markatou *et al.*, "Fe-Zeolite SCR model development, validation and application," in *SAE 2011 World Congress and Exhibition*, 2011. doi: 10.4271/2011-01-1304.
[22] T. Rammelt, A. B. Kuc, J. Böhm, T. Heine, and R. Gläser, "Nature and Surface Interactions of Sulfur-Containing Deposits on V2O5-WO3/TiO2 Catalysts for SCR-DeNOx," *Emission Control Science and Technology*, vol. 5, no. 4, pp. 297–306, Dec. 2019, doi: 10.1007/s40825-019-00142-1.
[23] M. Bendrich, A. Scheuer, R. E. Hayes, and M. Votsmeier, "Unified mechanistic model for Standard SCR, Fast SCR, and NO2 SCR over a copper chabazite catalyst," *Appl Catal B*, vol. 222, pp. 76–87, 2018, doi: 10.1016/j.apcatb.2017.09.069.
[24] M. Devarakonda, G. Parker, J. H. Johnson, V. Strots, and S. Santhanam, "Adequacy of Reduced Order Models for Model-Based Control in a Urea-SCR Aftertreatment System," 2008.
[25] T. Maunula, & M. Tuikka, and & T. Wolff, "The Reactions and Role of Ammonia Slip Catalysts in Modern Urea-SCR Systems", doi: 10.1007/s40825-020-00171-1/Published.
[26] A. Scheuer, W. Hauptmann, A. Drochner, J. Gieshoff, H. Vogel, and M. Votsmeier, "Dual layer automotive ammonia oxidation catalysts: Experiments and computer simulation," *Appl Catal B*, vol. 111–112, pp. 445–455, Jan. 2012, doi: 10.1016/j.apcatb.2011.10.032.
[27] N. Examiner, J. Sjöblom, A. Ghanaati, and E. Faghani, "Semi-Physical Modelling Approach for Exhaust Aftertreatment System of Heavy Duty Diesel Engines."
[28] "Gamma Technologies. Exhaust aftertreatment application manual. VERSION-2021".
[29] S. E. Vollz, C. R. Morgan, D. Liederman, and S. M. Jacob, "Downloaded via CLEMSON UNIV on," UTC, 1973. [Online]. Available: https://pubs.acs.org/sharingguidelines

[30] "Reaction Mechanism." https://chem.libretexts.org/Courses/New_York_University/CHEM-UA_652%3A_Thermodynamics_and_Kinetics/01%3A_Lectures/1.22%3A_Kinetics_of_Catalysis
[31] S. R. Gundlapally, R. Dudgeon, and S. Wahiduzzaman, "Efficient Solution of Washcoat Diffusion-Reaction Problem for Real-Time Simulations," *Emission Control Science and Technology*, vol. 4, no. 2, pp. 90–102, 2018, doi: 10.1007/s40825-018-0083-9.
[32] S. H. Oh, E. J. Bissett, and P. A. Battiston, "Mathematical Modeling of Electrically Heated Monolith Converters: Model Formulation, Numerical Methods, and Experimental Verification," 1993. [Online]. Available: https://pubs.acs.org/sharingguidelines
[33] S. Wahiduzzaman, W. Tang, and S. Wenzel, "Development and Application of a Fast Quasi-Steady Solver for Integrated Modeling of Exhaust Aftertreatment Systems."
[34] W. Tang, S. Wahiduzzaman, S. Wenzel, A. Leonard, and T. Morel, "Development of a Quasi-Steady Approach Based Simulation Tool for System Level Exhaust Aftertreatment Modeling," 2008.
[35] K. Deb and H. Jain, "An evolutionary many-objective optimization algorithm using reference-point-based nondominated sorting approach, Part I: Solving problems with box constraints," *IEEE Transactions on Evolutionary Computation*, vol. 18, no. 4, pp. 577–601, 2014, doi: 10.1109/TEVC.2013.2281535.
[36] J. Lock, K. Clasén, J. Sjöblom, and T. McKelvey, "Cold-Start Modeling and On-Line Optimal Control of the Three-Way Catalyst," Apr. 2021, [Online]. Available: http://arxiv.org/abs/2104.12390
[37] C. S. Sampara, E. J. Bissett, and M. Chmielewski, "Global kinetics for a commercial diesel oxidation catalyst with two exhaust hydrocarbons," *Ind Eng Chem Res*, vol. 47, no. 2, pp. 311–322, Jan. 2008, doi: 10.1021/ie070813x.
[38] D. M. Cavallo, O. Chiavola, and F. Palmieri, "Modelling of DOC Behavior under DPF Active Regeneration," in *SAE Technical Papers*, SAE International, Aug. 2022. doi: 10.4271/2022-01-1018.
[39] J. Luo *et al.*, "Effect of regeneration method and ash deposition on diesel particulate filter performance: a review," *Environmental Science and Pollution Research*, vol. 30, no. 16. Springer Science and Business Media Deutschland GmbH, pp. 45607–45642, Apr. 01, 2023. doi: 10.1007/s11356-023-25880-2.
[40] S. R. Christensen, B. B. Hansen, K. H. Pedersen, J. R. Thøgersen, and A. D. Jensen, "Selective Catalytic Reduction of NOx over V2O5-WO3-TiO2 SCR Catalysts—A Study at Elevated Pressure for Maritime Pre-turbine SCR Configuration," *Emission Control Science and Technology*, vol. 5, no. 3, pp. 263–278, Sep. 2019, doi: 10.1007/s40825-019-00127-0.
[41] P. S. Metkar, M. P. Harold, and V. Balakotaiah, "Experimental and kinetic modeling study of NH3-SCR of NOx on Fe-ZSM-5, Cu-chabazite and combined Fe- and Cu-zeolite monolithic catalysts," *Chem Eng Sci*, vol. 87, pp. 51–66, Jan. 2013, doi: 10.1016/j.ces.2012.09.008.

[42] P. S. Metkar, V. Balakotaiah, and M. P. Harold, “Experimental and kinetic modeling study of NO oxidation: Comparison of Fe and Cu-zeolite catalysts,” in *Catalysis Today*, Apr. 2012, pp. 115–128. doi: 10.1016/j.cattod.2011.11.032.

[43] M. Colombo, I. Nova, E. Tronconi, V. Schmeißer, B. Bandl-Konrad, and L. Zimmermann, “Experimental and modeling study of a dual-layer (SCR+PGM) NH3 slip monolith catalyst (ASC) for automotive SCR aftertreatment systems. Part 1. Kinetics for the PGM component and analysis of SCR/PGM interactions,” *Appl Catal B*, vol. 142–143, pp. 861–876, Oct. 2013, doi: 10.1016/j.apcatb.2012.10.031.

[44] M. Colombo, I. Nova, E. Tronconi, V. Schmeißer, B. Bandl-Konrad, and L. R. Zimmermann, “Experimental and modeling study of a dual-layer (SCR+PGM) NH3 slip monolith catalyst (ASC) for automotive SCR after treatment systems. Part 2. Validation of PGM kinetics and modeling of the dual-layer ASC monolith,” *Appl Catal B*, vol. 142–143, pp. 337–343, Oct. 2013, doi: 10.1016/j.apcatb.2013.05.032.

[45] M. Colombo, G. Koltsakis, I. Nova, and E. Tronconi, “Modelling the ammonia adsorption-desorption process over an Fe-zeolite catalyst for SCR automotive applications,” in *Catalysis Today*, Jul. 2012, pp. 42–52. doi: 10.1016/j.cattod.2011.09.002.

[46] J. M. Kanervo, S. Kouva, K. J. Kanervo, R. Kolvenbach, A. Jentys, and J. A. Lercher, “Prerequisites for kinetic modeling of TPD data of porous catalysts-Exemplified by toluene/H-ZSM-5 system,” *Chem Eng Sci*, vol. 137, pp. 807–815, Dec. 2015, doi: 10.1016/j.ces.2015.07.032.

[47] J. Kanervo, T. J. Keskitalo, R. I. Slioor, and A. Krause, “Temperature-programmed desorption as a tool to extract quantitative kinetic or energetic information for porous catalysts,” *J Catal*, vol. 238, pp. 382–393, Mar. 2006, doi: 10.1016/j.jcat.2005.12.026.

[48] B. Environmental and H. J. Stein, “Diesel oxidation catalysts for commercial vehicle engines: strategies on their application for controlling particulate emissions,” 1996.

[49] X. Wang, G. Song, Y. Wu, L. Yu, and Z. Zhai, “A NOx emission model incorporating temperature for heavy-duty diesel vehicles with urea-SCR systems based on field operating modes,” *Atmosphere (Basel)*, vol. 10, no. 6, Jun. 2019, doi: 10.3390/atmos10060337.

[50] Y. Cui and F. Gao, “Cu Loading Dependence of Fast NH3-SCR on Cu/SSZ-13,” *Emission Control Science and Technology*, vol. 5, no. 2, pp. 124–132, 2019, doi: 10.1007/s40825-019-00117-2.